

Laplacian Representations for Decision-Time Planning

Dikshant Shehmar^{1,2} Matthew Schlegel³ Matthew E. Taylor^{1,2,4} Marlos C. Machado^{1,2,4}

Abstract

Planning with a learned model remains a key challenge in model-based reinforcement learning (RL). In decision-time planning, state representations are critical as they must support local cost computation while preserving long-horizon structure. In this paper, we show that the Laplacian representation provides an effective latent space for planning by capturing state-space distances at multiple time scales. This representation preserves meaningful distances and naturally decomposes long-horizon problems into subgoals, also mitigating the compounding errors that arise over long prediction horizons. Building on these properties, we introduce ALPS, a hierarchical planning algorithm, and demonstrate that it outperforms commonly used baselines on a selection of offline goal-conditioned RL tasks from OGBench, a benchmark previously dominated by model-free methods.

1. Introduction

Compared to model-free reinforcement learning (RL), model-based RL offers, among other benefits, the potential for improved sample efficiency (Janner et al., 2019; Wang et al., 2019), better generalization (Deisenroth & Rasmussen, 2011; Yu et al., 2020), and faster adaptation (Zhang et al., 2020; Wan et al., 2022). These gains stem from the agent’s ability to use a model to reason about consequences before acting, a process known as planning (Sutton, 1991). Nevertheless, when function approximation is required, planning with a *learned model* remains a central challenge, due to both how states are represented in latent space and generalize, and to the well-known problem of compounding errors over long sequences of predictions (Talvitie, 2014; 2017; Venkatraman et al., 2015; Clavera et al., 2018).

¹Dept. of Computing Science, University of Alberta, Canada
²Alberta Machine Intelligence Institute (Amii)
³Schulich School of Engineering, Dept. of Electrical and Software Engineering, University of Calgary, Canada
⁴Canada CIFAR AI Chair, Amii
Correspondence to: Dikshant Shehmar <ddikshan@ualberta.ca>.

Preprint. February 6, 2026.

Decision-time planning algorithms such as MPC (García et al., 1989) and MCTS (Kocsis & Szepesvári, 2006) use the model to choose actions based on simulated future trajectories and predicted outcomes. In this setting, the effects of compounding errors over long horizons due to imperfect models become obvious when imagined trajectories diverge from reality (Gu et al., 2016; Lambert et al., 2022). Hierarchical planning can overcome this limitation by decoupling the agent’s low-level actions from its long-horizon objectives (Koul et al., 2024), but requires a latent space in which to plan at long time scales. State representation is therefore critical: nearby states must be close in latent space, while long-term distances must also be preserved to support planning toward a desired goal.

The Laplacian representation (Mahadevan, 2005; Mahadevan & Maggioni, 2007) embeds states into a latent space defined by the eigenvectors of the graph Laplacian induced by the environment’s dynamics. It captures the environment’s temporal structure and connectivity, with eigenvectors ordered by time scale: early eigenvectors encode global structure (e.g., rooms or regions), while later ones capture increasingly local distinctions (Machado et al., 2017; 2023; Jinnai et al., 2019; 2020). Because this representation reflects reachability, it naturally partitions the environment into well-connected regions (Shi & Malik, 2000). Moreover, Euclidean distance in the Laplacian space approximates how easily one state can be reached from another by following the environment’s dynamics (Lovász et al., 1993), yielding a geometry well suited for planning. As a result, in this paper, we show how the Laplacian representation supports both subgoal discovery and planning in a unified metric space.

This paper tackles decision-time planning with a learned model in environments requiring function approximation. We show that the Laplacian representation provides an effective latent space for planning by intrinsically capturing multiple time scales. We further demonstrate that hierarchical planning enables decision-time planning in long-horizon tasks, with the Laplacian representation decomposing tasks into subgoals. We instantiate these ideas in a novel hierarchical decision-time planning algorithm, Augmented Laplacian Planning with Subgoals (ALPS), where the Laplacian representation supports both subgoal identification and distance estimation. Empirically, ALPS outperforms the commonly used model-free RL baselines on a suite of goal-conditioned

tasks from OGBench (Park et al., 2025).

2. Preliminaries

In this paper, we use lowercase symbols (e.g., r) for functions and values of random variables, uppercase symbols (e.g., C) for constants and random variables, calligraphic font (e.g., \mathcal{S}) for sets, bold lowercase symbols (e.g., \mathbf{e}) for vectors, and bold uppercase symbols (e.g., \mathbf{L}) for matrices. We write the i -th entry of a vector \mathbf{v} as $\mathbf{v}(i)$.

2.1. Problem Setting

We consider the offline Goal-Conditioned Reinforcement Learning (GCRL) setting (Kaelbling, 1993; Liu et al., 2022). The agent-environment interaction is modeled as a goal-augmented Markov decision process (GA-MDP), $\mathcal{M} = \langle \mathcal{S}, \mathcal{A}, \mathbf{P}, \mu, \gamma, \mathcal{G} \rangle$ where \mathcal{S} and \mathcal{A} denote the state and action spaces respectively, \mathbf{P} denotes the state transition dynamics (where $\mathbf{P}(s'|s, a)$ is the probability of transitioning from s to s'), μ is the initial state distribution, $\gamma \in [0, 1]$ is the discount factor, and the goal space $\mathcal{G} \subseteq \mathcal{S}$ is the same as the state space. A dataset \mathcal{D} is provided consisting of trajectories $\tau^{(n)} = (S_0^{(n)}, A_0^{(n)}, S_1^{(n)}, \dots, S_T^{(n)})$ sampled from the environment through a preset behavior policy. The agent aims to learn a goal-conditioned policy $\pi(a|s, g) : \mathcal{S} \times \mathcal{G} \rightarrow \Delta(\mathcal{A})$ that maximizes the objective:

$$\mathbb{E}_{\tau \sim \mathbf{P}_\tau(\tau|g)} \left[\sum_{t=0}^T \gamma^t r(S_t, g) \right] \forall g \in \mathcal{G},$$

where $r(S_t, g)$ is a sparse reward function (e.g., an indicator $\mathbb{I}[S_t = g]$), $T \in \mathbb{N}$ denotes the episode length, and \mathbf{P}_τ is the distribution of seeing a trajectory with respect to a policy π and a goal g (Park et al., 2025). $\mathbf{P}_\pi(s'|s) = \sum_{a \in \mathcal{A}} \pi(a|s, g) \mathbf{P}(s'|s, a)$ is the state-transition distribution under policy π .

2.2. Laplacian Representation in RL

The Laplacian framework (Mahadevan, 2005; Mahadevan & Maggioni, 2007) proposes a state representation that reflects global geometries of a Markov decision process (MDP) leveraging spectral analysis. The states and transitions of an MDP are re-interpreted as nodes and edges in a weighted graph $G = (\mathcal{S}, \mathcal{E})$, where $(i, j) \in \mathcal{E}$ if the agent can observe the transition $s_i \rightarrow s_j$ in a single step and edge weights are determined by the transition matrix \mathbf{P}_π induced by the policy π . The graph Laplacian \mathbf{L} can be defined with respect to a policy π as

$$\mathbf{L} = \mathbf{I} - f(\mathbf{P}_\pi),$$

where \mathbf{I} is the identity matrix, and f is a symmetrization function, for example, $f(\mathbf{P}_\pi) = \frac{1}{2}(\mathbf{P}_\pi + \mathbf{P}_\pi^\top)$ (Wu et al., 2019). Since \mathbf{L} is a real symmetric matrix, its eigendecomposition is $\mathbf{L} = \mathbf{E} \Lambda \mathbf{E}^\top$, where $\mathbf{E} = [\mathbf{u}_0, \mathbf{u}_1, \dots, \mathbf{u}_{|\mathcal{S}|}]$ have

eigenvectors as columns, and $\Lambda = \text{diag}(\lambda_0, \lambda_1, \dots, \lambda_{|\mathcal{S}|})$ contains the corresponding eigenvalues.

The *Laplacian representation* is a state representation mapping $\phi : \mathcal{S} \rightarrow \mathbb{R}^D$ ($0 < D \leq |\mathcal{S}|$) defined by the eigenvectors of \mathbf{L} corresponding to the smallest D non-zero eigenvalues (Mahadevan, 2005; Gomez et al., 2023). ¹ The first eigenvector, \mathbf{u}_0 , is constant and uninformative, and thus is discarded.

Recently, several methods have been proposed to learn the Laplacian representation from samples. This overcomes the high computational barrier, i.e. $O(|\mathcal{S}|^3)$, of performing an eigendecomposition on the graph Laplacian. We use Augmented Lagrangian Laplacian Objective (ALLO; Gomez et al., 2023), an objective to learn the eigenvectors and eigenvalues of the graph Laplacian:

$$\begin{aligned} \max_{\beta} \min_{\mathbf{U}} \sum_{i=1}^D \langle \mathbf{u}_i, \mathbf{L} \mathbf{u}_i \rangle + \sum_{j=1}^D \sum_{k=1}^j \beta_{jk} (\langle \mathbf{u}_j, [\mathbf{u}_k] \rangle - \delta_{jk}) \\ + B \sum_{j=1}^D \sum_{k=1}^j (\langle \mathbf{u}_j, [\mathbf{u}_k] \rangle - \delta_{jk})^2, \quad (1) \end{aligned}$$

where $\mathbf{u}_i \in \mathbb{R}^{|\mathcal{S}|}$ denotes the i -th learned eigenvector, $(\beta_{jk})_{1 \leq k \leq j \leq D}$ are the corresponding dual variables that enforce orthonormality, $\lambda_i = -\beta_{ii}/2$ are the eigenvalues, δ_{jk} is the Kronecker delta, and B is the barrier coefficient.²

2.3. Planning with a learned model

Model Predictive Control (MPC) is a common approach for planning in continuous action spaces. In MPC, a model is used to select the greedy action from a k -step lookahead search with respect to a cost function; the greedy action is then executed, and the process is repeated using the new state. The Cross-Entropy Method (CEM; Rubinstein, 1997) is a popular MPC-based planner that has been successful in model-based RL settings (Finn & Levine, 2017; Chua et al., 2018; Hafner et al., 2019; Pinneri et al., 2021; Görtler & Martius, 2025). CEM samples action sequences using a diagonal Gaussian, $\mathbf{a}_{t:t+H} \sim \mathcal{N}(\boldsymbol{\mu}_{t:t+H}, \text{diag}(\boldsymbol{\sigma}_{t:t+H}^2))$, and rolls them out using a forward model. Based on the top- N_e trajectories with the lowest cost to the goal, the mean $\boldsymbol{\mu}$ and variance $\boldsymbol{\sigma}^2$ are updated accordingly. MPC works reliably, provided that the planning horizon remains within the model's accuracy window (Chua et al., 2018; Feinberg et al., 2018). As the planning horizon increases, the model error quickly compounds, making the planning signal unreliable.

Hierarchical planning has the potential to solve the com-

¹We define the Laplacian representation in the discrete setting for simplicity, but a principled analogous version exists for continuous state spaces (Gomez et al., 2023).

²Gomez et al. (2023) shows that ALLO is insensitive to the value of the barrier coefficient, which has also been our experience.

pounding error issue by decomposing the original problem into smaller subproblems with a shorter horizon. One example of a hierarchical decision-time planning algorithm is Plannable Continuous Latent States (PcLast; [Koul et al., 2024](#)). PcLast works by constructing a high-level and low-level latent space. The low-level latent space is learned through the Agent-Controller Representations (ACRO; [Islam et al., 2023](#)) objective. The high-level latent space, using the low-level latent space as input, is constructed based on the likelihood of a random walk reaching state s_{t+k} from s_t and is learned through a contrastive objective (see Appendix B.1 for details). The high-level latent space is then used to generate a graph of subgoals, defined as the centroids obtained through k -means. PcLast then performs low-level planning between subgoals in the low-level latent space using CEM, with a cost function defined in the high-level latent space. ALPS is heavily inspired by PcLast, but instead uses the Laplacian representation as its high-level latent space to capture environment geometry directly from the raw state space, and includes a behavior prior to bias CEM optimization.

3. The Laplacian for Long-Horizon Planning

In this section, we motivate the Laplacian representation as an ideal latent space for both a high-level and low-level planner. The Laplacian representation naturally lends itself as a latent space for hierarchical planning. The representation induces a metric space that encodes the environment’s temporal structure and connectivity at multiple time scales. Furthermore, Laplacian representations act as a natural basis for a set of clustering methods that are well-suited for subgoal identification ([Şimşek et al., 2005](#); [Von Luxburg, 2007](#)). Finally, as discussed in Section 2.2, recent breakthroughs in learning the Laplacian representation from data ([Wu et al., 2019](#); [Wang et al., 2021](#); [Gomez et al., 2023](#)) unlock the aforementioned benefits in problems with large state and action spaces.

The distance metric induced by the Laplacian representation has a well known connection to commute time distance (CTD).³ CTD $c(u, v)$ is defined as the expected number of steps to travel from node u to v and back following a random walk ([Lovász et al., 1993](#)). The eigenvectors and eigenvalues of the graph Laplacian can be used to calculate the CTD directly:

$$c(u, v) = \text{vol}(G) \sum_{i=1}^{|S|} \left(\frac{\mathbf{u}_i(u)}{\sqrt{\lambda_i}} - \frac{\mathbf{u}_i(v)}{\sqrt{\lambda_i}} \right)^2,$$

where $\text{vol}(G)$ is the volume of the graph ([Xiao & Gutman, 2003](#); [Wang et al., 2023a](#)). To take advantage of this relation,

³The resistance distance, $r_d(u, v) = \frac{c(u, v)}{\text{vol}(G)}$ ([Klein & Randić, 1993](#)), can equivalently be used.

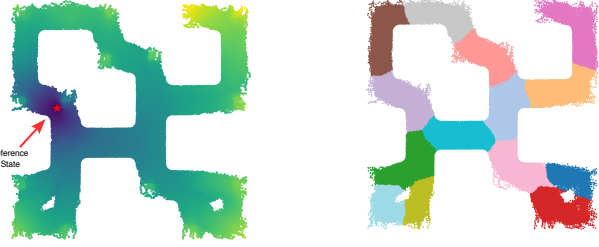


Figure 1. Visualization of the ψ -space properties in the *pointmaze-medium* maze environment from OGBench. (left) Heatmap of $c(s^*, s_i)$ distance from a reference state (s^* denoted by \star in the figure) to each state in the dataset. (right) Cluster labels assigned to each state in the dataset via clustering in ψ -space.

the scaled Laplacian representation⁴ $\psi_i(s) = \phi_i(s)/\sqrt{\lambda_i}$ is used to approximate CTD $c(s_u, s_v) \approx \|\psi(u) - \psi(v)\|^2$. For completeness, we provide a derivation of this approximation in Appendix A.1. We refer to the scaled Laplacian space induced by ALLO as ψ -space. Since the ψ -space is isometric to the reachability information, it acts as an ideal space for low-level planning.

Spectral clustering consists of using the Laplacian representation as a basis for clustering ([Weiss, 1999](#); [Ng et al., 2001](#); [Von Luxburg, 2007](#)). Intuitively, from the perspective of CTD, clustering using the Laplacian representation as a basis partitions the environment at its bottlenecks and groups well-connected regions ([Shi & Malik, 2000](#)). A random walk on the graph is unlikely to travel between different clusters, and in the Laplacian representation this is reflected in a longer distance between points from different clusters. Using the scaled Laplacian representation accentuates the relationships between points compared to the non-scaled version, pulling similar points closer together and pushing dissimilar points further apart ([Qiu & Hancock, 2007](#)). Motivated by these properties, we use the scaled Laplacian representation as a latent space for subgoal identification through k -means clustering, and perform high-level planning in this ψ -space.

So far, we have motivated the scaled Laplacian representation as an ideal latent space for hierarchical planning by connecting it to CTD and spectral clustering. In Figure 1, we visualize the Laplacian representation learned with ALLO in the *medium pointmaze* environment from OGBench (see Section 5 for more details). Note that (1) the approximation of CTD shows distances that are temporally consistent, and (2) the tight clusters that respect the environment dynamics whose centers can be used as subgoals. These characteristics of the scaled Laplacian representation provide a strong foundation for hierarchical decision-time planning.

⁴We call this the scaled Laplacian representation, but it has several names throughout the literature, such as reachability-aware Laplacian representation ([Wang et al., 2023a](#)), and commute-embedding ([Qiu & Hancock, 2007](#)).

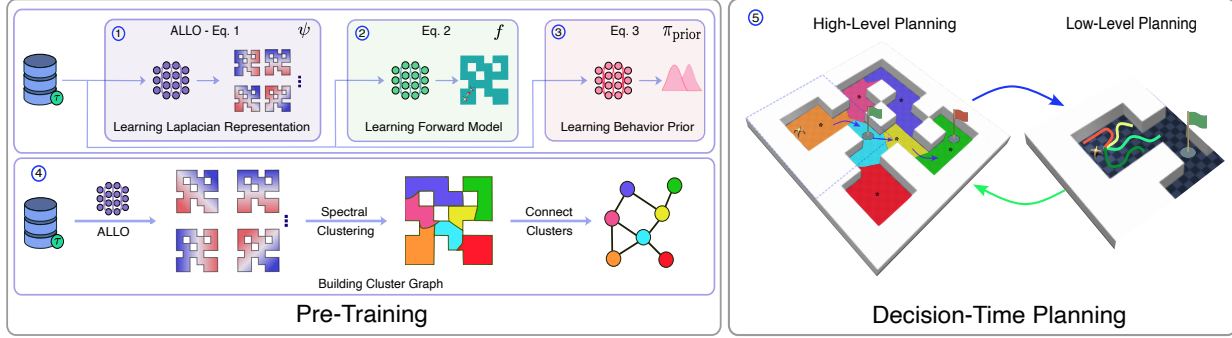


Figure 2. ALPS at the pre-training and decision-time planning phases. In pre-training, ALPS (1) learns the Laplacian representation using Augmented Lagrangian Laplacian Objective (ALLO), (2) learns a one-step forward model on-top of the original state space \mathcal{S} , (3) learns the behavior prior π_{prior} using the scaled Laplacian representation, and (4) clusters the dataset using k -means in the scaled Laplacian space to generate the cluster graph. In planning, (5) ALPS takes the current state from the environment and uses the high-level planner to determine the next subgoal, and then determines the next action towards this subgoal using the low-level planner.

4. Augmented Laplacian Planning with Subgoals

Augmented Laplacian Planning with Subgoals (ALPS) is a model-based hierarchical planning algorithm that leverages the Laplacian representation to efficiently plan in continuous state and action spaces. ALPS leverages an offline dataset to learn: (1) the Laplacian representation, (2) a forward model, and (3) a behavior prior. Clustering is then performed over the scaled Laplacian representation as a basis, and the clusters centers are used as subgoals. When given a goal state, a high-level plan over subgoals is constructed using Dijkstra algorithm and this plan is executed using CEM with a behavior prior guiding its search. ALPS is outlined in Algorithm 1 with its components detailed in Fig. 2.

Learning the Laplacian representation: We learn the Laplacian representation using the ALLO objective (Eq. 1). The ALLO objective is minimized using stochastic gradient descent by sampling transition pairs $(S_t, S_{t+\Delta})$, where $\Delta \sim \text{Geom}(1 - \gamma_s)$ is the geometric distribution.

Learning a forward model: The low-level planner uses a one-step model in the original state space $f : \mathcal{S} \times \mathcal{A} \rightarrow \mathcal{S}$. To reduce the accumulation of errors known to occur in one-step forward models, we use a multi-step auto-regressive objective over the horizon H_f (Talvitie, 2014; 2017):

$$\mathbb{E}_{(S_t, A_{t:t+H_f-1}, S_{t+1:t+H_f}) \sim \mathcal{D}} \left[\frac{1}{H_f} \sum_{\tau=1}^{H_f} \|\hat{S}_{t+\tau} - S_{t+\tau}\|_2^2 \right], \quad (2)$$

where $\hat{S}_{t+1} = f(S_t, A_t)$ and $\hat{S}_{t+\tau} = f(\hat{S}_{t+\tau-1}, A_{t+\tau-1})$ for $\tau > 1$. Auto-regressive training allows gradients to flow back through time (Werbos, 1990), incentivizing the model to learn transition dynamics that remain stable over H_f .

Learning a behavior prior: Usually, CEM samples action sequences from an unconditional Gaussian distribu-

tion, but this strategy is inefficient for high-dimensional action spaces (Bharadhwaj et al., 2020). To accelerate the convergence of CEM, we use a behavior prior to generate candidate action sequences (Hansen et al., 2024). The behavior prior, $\pi_{\text{prior}}(S_t, \psi(S_t), \psi(S_{t+k}))$ is a deterministic goal-conditioned policy. We learn π_{prior} by minimizing

$$\mathbb{E}_{(S_t, A_t, S_{t+k}) \sim \mathcal{D}} [\|\pi_{\text{prior}}(S_t, \psi(S_t), \psi(S_{t+k})) - A_t\|_2^2], \quad (3)$$

where $k \sim U(1, K_{\text{max}})$, with K_{max} as a hyperparameter. This behavior cloning objective encourages goal-directed behavior by assuming all trajectories in the dataset are generated by a goal-seeking policy trying to reach the goal state S_{t+k} from S_t . The behavior prior is then used to predict an action sequence $\mathbf{a}_{t:t+H-1}$ from a state S_t using the forward model over the planner horizon H .

Building a Cluster Graph: The space is partitioned into C regions $\{c_i\}_{i=1}^C$ using k -means clustering in the ψ -space. The cluster centers acts as the vertices of a graph G_c , with the edges defined by the dataset \mathcal{D} : an edge (i, j) exists if we observe transitions from states that belong to cluster i to states from cluster j (or the converse). Like PCLast, we use nucleus sampling (Holtzman et al., 2020) to remove infrequent transitions between the clusters to avoid subgoals that are too hard to reach.

Decision-time Planning: At the beginning of an episode, the planner receives the start state s_{start} and the goal state s_{goal} . It then identifies their respective clusters, c_s and c_g , in the cluster graph G_c . Dijkstra's algorithm (Dijkstra, 1959) finds the shortest path \mathcal{P}_G on the cluster graph between the clusters c_s and c_g . \mathcal{P}_G acts as a high-level plan for the agent, providing a path in the scaled Laplacian ψ -space.

At each step of the episode, the high-level planner provides the next target cluster center z_{sub} from \mathcal{P}_G . Using the next target cluster and the agent's current state, CEM uses the behavior prior π_{prior} to generate an action sequence $\mathbf{a}_{t:t+H-1}$

Algorithm 1 ALPS

Training Input: Dataset \mathcal{D} , # eigenvectors D , # clusters C
 === Pre-Training Phase ===
 $\psi \leftarrow \text{TrainALLO}(\mathcal{D})$ $\triangleright \psi : \mathcal{S} \rightarrow \mathbb{R}^d$
 $f \leftarrow \text{TrainDynamics}(\mathcal{D})$ $\triangleright f : \mathcal{S} \times \mathcal{A} \rightarrow \mathcal{S}$
 $\pi_{\text{prior}} \leftarrow \text{TrainBehaviorPrior}(\mathcal{D}, \psi)$ $\triangleright \pi_{\text{prior}} : \mathcal{S} \times \psi \times \psi \rightarrow \mathcal{A}$
 === Get Cluster Graph ===
 $\text{labels} \leftarrow \text{KMeans}(\psi(\mathcal{D}), C)$
 $G_c \leftarrow \text{BuildClusterGraph}(\mathcal{D}, \text{labels})$
 === Decision-Time Planning ===
Testing Input: $s_{\text{start}}, s_{\text{goal}}$ \triangleright get start and goal state
 $z_s \leftarrow \psi(s_{\text{start}}), z_g \leftarrow \psi(s_{\text{goal}})$
 $c_s \leftarrow \text{getCluster}(z_s), c_g \leftarrow \text{getCluster}(z_g)$ \triangleright get cluster label
 $\mathcal{P}_G \leftarrow \text{Dijkstra}(G_c, c_s, c_g)$ \triangleright get high-level plan
 $i \leftarrow 1$ \triangleright index of next target cluster
while $\|\psi(s) - z_g\| > \epsilon$ **do**
 $c_{\text{curr}} \leftarrow \text{getCluster}(\psi(s))$
if $c_{\text{curr}} \notin \mathcal{P}_G$ **then**
 $\mathcal{P}_G \leftarrow \text{Dijkstra}(G_c, c_{\text{curr}}, c_g)$ \triangleright replan if drifted from \mathcal{P}_G
 $i \leftarrow 1$
else if $c_{\text{curr}} = \mathcal{P}_G[i]$ **then**
 $i \leftarrow \min(i + 1, |\mathcal{P}_G| - 1)$ \triangleright advance if reached target
end if
 $z_{\text{sub}} \leftarrow \begin{cases} z_g & \text{if } \mathcal{P}_G[i] = c_g \\ \text{centroid}(\mathcal{P}_G[i]) & \text{otherwise} \end{cases}$
 $\mathbf{a} \leftarrow \text{CEM}(s, z_{\text{sub}}, \psi, f, \pi_{\text{prior}})$
 $s \leftarrow \text{env.step}(\mathbf{a}_1)$
end while

for a horizon H . Temporally-correlated Gaussian noise σ is added around the action sequence $\mathbf{a}_{t:t+H-1}$ to generate N_s candidate action sequences (Wang & Ba, 2020). The action sequences are passed to the forward model to generate multiple trajectories. Each trajectory j is then evaluated using the cost function

$$J^j \leftarrow \sum_{t=1}^H \left(\|\psi(\hat{S}_t^j) - z_{\text{sub}}\|_2^2 + \lambda \|A_t^j\|_2^2 \right), \quad (4)$$

where the first term minimizes the distance in Laplacian space and the second term penalizes large actions with λ as a hyperparameter. We penalize extreme actions to prevent abrupt behavior. Note that since we perform spectral clustering in ψ -space, the distance between $\psi(\hat{S}_t)$ and z_{sub} approximates the CTD between corresponding states. The top- N_e lowest cost trajectories are then used to update the sampling distribution, and this process is repeated over N_{iter} iterations. The agent then executes the first action of the best action sequence. If the agent deviates from the precomputed plan, the high-level planner recomputes a plan from the current cluster to the goal state.

Once the agent enters the current target cluster, the next cluster center in \mathcal{P}_G becomes the target cluster. This process repeats until the agent reaches the goal cluster, when CEM uses the goal state as the final target. The pseudocode of the CEM planner is outlined in Appendix C.

5. Experiments

We now empirically validate the utility of the Laplacian representation as a latent space for decision-time planning with ALPS. First, given that ALPS shares many of the same components as PcLast, we directly compare these algorithms on Maze2D—Point Mass tasks, where PcLast was originally evaluated. These environments pose difficult navigation conditions for long-horizon planning and state-space partitioning from images, as they require the agent to travel far to reach states that appear close in Euclidean space.

To demonstrate ALPS’ scalability and potential, we then evaluate it in tasks with much larger state and action spaces. We do so by using locomotion tasks from Offline-Goal Conditioned RL Benchmark suite (OGBench), a complex robotic benchmark for comparing offline GCRL algorithms. These tasks are difficult not only because navigating from start to goal requires navigating a maze, but because the underlying locomotion is itself challenging. Up-to-now, model-free baselines have led performance across all OGBench tasks.

5.1. Methodology

In all environments, performance is measured by the percent success of navigating between start and goal states from a test set within a set number of interactions with the environment. Unless otherwise specified, all results report mean and standard deviation over 8 random trials. Hyperparameter details are in Appendix E.

Maze2D—PointMass (Koul et al., 2024): Each maze is a unit square with varied wall configurations (see Figure 4 in Appendix D.1). The agent controls a point mass with actions corresponding to the coordinate space change $(\Delta x, \Delta y)$ bounded by the range $[-0.2, 0.2]$ for each action. Observations are defined as a single-channel (100×100) image encoding the current position of the agent and no other environmental information. A Gaussian blur ($\sigma = 1.0$) is applied to the agent’s coordinate position, and the resulting image is normalized to $[0, 1]$. An offline dataset of $500K$ transitions is generated using a uniform random policy. We follow PcLast’s empirical design where the agent must navigate from a starting position to within 0.03 units of a known target position within 30 actions.

Locomotion tasks from OGBench (Park et al., 2025): We use three locomotion tasks from OGBench: *pointmaze*, *antmaze*, and *humanoidmaze*. They require controlling 2-DoF, 8-DoF, and 21-DoF bodies, respectively. The dataset types are as follows: (i) *navigate*, collected by a noisy expert policy that navigates the maze by repeatedly reaching randomly sampled goals; (ii) *stitch*, collected through shorter goal-reaching trajectories from a noisy expert, which test the agent’s stitching ability; and (iii) *explore*, collected

Table 1. Success rate (%) on each of the locomotion tasks from OGBench considered. The results are averaged over 8 seeds, and we report the standard deviation after the \pm sign. ALPS outperforms the model-free GCRL algorithms with $p < 0.01$ using a Holm-Bonferroni-corrected two-sided Wilcoxon signed-rank test. Values in **bold** denote the largest mean in each row as a visual aid.

Environment	Dataset	Dataset Type	GCBC	GCIVL	GCIQL	QRL	CRL	HIQL	ALPS
pointmaze	navigate	pointmaze-medium-navigate-v0	9 \pm 6	63 \pm 6	53 \pm 8	82 \pm 5	29 \pm 7	79 \pm 5	82 \pm 10
		pointmaze-large-navigate-v0	29 \pm 6	45 \pm 5	34 \pm 3	86 \pm 9	39 \pm 7	58 \pm 5	76 \pm 7
		pointmaze-giant-navigate-v0	1 \pm 2	0 \pm 0	0 \pm 0	68 \pm 7	27 \pm 10	46 \pm 9	65 \pm 9
	stitch	pointmaze-teleport-navigate-v0	25 \pm 3	45 \pm 3	24 \pm 7	4 \pm 4	24 \pm 6	18 \pm 4	40 \pm 4
		pointmaze-medium-stitch-v0	23 \pm 18	70 \pm 14	21 \pm 9	80 \pm 12	0 \pm 1	74 \pm 6	90 \pm 7
		pointmaze-large-stitch-v0	7 \pm 5	12 \pm 6	31 \pm 2	84 \pm 15	0 \pm 0	13 \pm 6	96 \pm 2
antmaze	navigate	pointmaze-giant-stitch-v0	0 \pm 0	0 \pm 0	0 \pm 0	50 \pm 8	0 \pm 0	0 \pm 0	99 \pm 1
		pointmaze-teleport-stitch-v0	31 \pm 9	44 \pm 2	25 \pm 3	9 \pm 5	4 \pm 3	34 \pm 4	20 \pm 5
		antmaze-medium-navigate-v0	29 \pm 4	72 \pm 8	71 \pm 4	88 \pm 3	95 \pm 1	96 \pm 1	95 \pm 4
		antmaze-large-navigate-v0	24 \pm 2	16 \pm 5	34 \pm 4	75 \pm 6	83 \pm 4	91 \pm 2	94 \pm 3
	stitch	antmaze-giant-navigate-v0	0 \pm 0	0 \pm 0	0 \pm 0	14 \pm 3	16 \pm 3	65 \pm 5	68 \pm 5
		antmaze-teleport-navigate-v0	26 \pm 3	39 \pm 3	35 \pm 5	35 \pm 5	53 \pm 2	42 \pm 3	44 \pm 5
		antmaze-medium-stitch-v0	45 \pm 11	44 \pm 6	29 \pm 6	59 \pm 7	53 \pm 6	94 \pm 1	95 \pm 4
		antmaze-large-stitch-v0	3 \pm 3	18 \pm 2	7 \pm 2	18 \pm 2	11 \pm 2	67 \pm 5	95 \pm 2
explore	navigate	antmaze-giant-stitch-v0	0 \pm 0	0 \pm 0	0 \pm 0	0 \pm 0	0 \pm 0	2 \pm 2	92 \pm 2
		antmaze-teleport-stitch-v0	31 \pm 6	39 \pm 3	17 \pm 2	24 \pm 5	31 \pm 4	36 \pm 2	34 \pm 9
		antmaze-medium-explore-v0	2 \pm 1	19 \pm 3	13 \pm 2	1 \pm 1	3 \pm 2	37 \pm 10	100 \pm 1
	explore	antmaze-large-explore-v0	0 \pm 0	10 \pm 3	0 \pm 0	0 \pm 0	0 \pm 0	2 \pm 2	91 \pm 13
		antmaze-teleport-explore-v0	2 \pm 1	32 \pm 2	7 \pm 3	2 \pm 2	20 \pm 2	34 \pm 15	46 \pm 6
		humanoidmaze-medium-navigate-v0	8 \pm 2	24 \pm 2	27 \pm 2	21 \pm 8	60 \pm 4	89 \pm 2	86 \pm 6
humanoidmaze	navigate	humanoidmaze-large-navigate-v0	1 \pm 0	2 \pm 1	2 \pm 1	5 \pm 1	24 \pm 4	49 \pm 4	54 \pm 5
		humanoidmaze-giant-navigate-v0	0 \pm 0	0 \pm 0	0 \pm 0	1 \pm 0	3 \pm 2	12 \pm 4	64 \pm 9
	stitch	humanoidmaze-medium-stitch-v0	29 \pm 5	12 \pm 2	12 \pm 3	18 \pm 2	36 \pm 2	88 \pm 2	62 \pm 6
		humanoidmaze-large-stitch-v0	6 \pm 3	1 \pm 1	0 \pm 0	3 \pm 1	4 \pm 1	28 \pm 3	35 \pm 5
		humanoidmaze-giant-stitch-v0	0 \pm 0	0 \pm 0	0 \pm 0	0 \pm 0	0 \pm 0	3 \pm 2	38 \pm 8

by commanding the low-level policy with a large amount of action noise, aimed to test agent's navigation skills from an extremely low-quality (yet high-coverage) data. An episode is terminated as soon as the agent reaches within the proximity of the goal location or the step limit is reached, which varies for different environments. The performance of each agent is averaged over 750 rollouts (3 evaluation epochs \times 5 test-time goals \times 50 rollouts). See Appendix D.2 for further details about environments and evaluation setup.

We compare to the baseline algorithms selected by Park et al. (2025): goal-conditioned behavior cloning (GCBC; Lynch et al., 2020; Ghosh et al., 2021), goal-conditioned implicit {V, Q}-learning (GCIVL; Kostrikov et al., 2022), (GCIQL; Park et al., 2024a), quasimetric RL (QRL; Wang et al., 2023b), contrastive RL (CRL; Eysenbach et al., 2022), and hierarchical implicit Q-learning (HIQL; Park et al., 2023).

5.2. Comparison with PcLast

ALPS differs from PcLast by the latent space used for the high-level planner and for trajectory optimization, as well as by the fact that ALPS uses a behavior prior to accelerate planner convergence. To evaluate the impact of using different latent spaces, isolating the impact of the representation used, we compare the performance of PcLast to ALPS when not using a behavior prior, which we denote by ALPS † . We consider two scenarios, one with only the low-level planner, using a single cluster, and one with the high-level planner, using 16 clusters. The results are shown in Table 2.

Overall, ALPS † outperforms PcLast in both scenarios. Both algorithms perform better across all domains when using

Table 2. Success rate (%) of PcLast and ALPS † on the Maze2D—PointMass environments. Mean and std. deviation over 10 seeds.

Environment	Clusters	PcLast	ALPS †
Hallway	1	51 \pm 4	98 \pm 1
	16	62 \pm 4	99 \pm 1
Rooms	1	30 \pm 3	84 \pm 5
	16	57 \pm 10	96 \pm 5
Spiral	1	35 \pm 4	93 \pm 3
	16	60 \pm 6	97 \pm 2

both the high- and low-level planners jointly, demonstrating that they learn a latent space useful for planning. Our distance metric's ability to disentangle the state space with respect to the dynamics can be clearly seen in the Spiral domain when the high-level planner is not included, resulting in similar performance in the low- and high-level settings with ALPS † . PcLast, however, has a substantial performance reduction when not using the high-level planner in Spiral. The above results demonstrate the scaled Laplacian representation's utility as both a distance metric for the low-level planner and a latent representation for subgoal identification through spectral clustering.

5.3. Scaling to large state and action spaces

We now empirically demonstrate that ALPS also scales to large state and action spaces. The results are reported in Table 1. ALPS significantly outperforms the baselines across domains according to a two-sided paired Wilcoxon signed-rank test applied to per-domain mean performance, with Holm-Bonferroni correction $p < 0.01$; see Appendix E.1

Table 3. Success rates (%) for the six variants of ALPS compared in Section 6 on a subset of the OGBench tasks considered. Results are averaged over 8 seeds with the standard deviation after the \pm sign. CEM, π_{prior} , and CEM + π_{prior} use only low-level planning. Dijkstra + CEM and Dijkstra + π_{prior} are the hierarchical planning variants with either CEM or π_{prior} acting as the low-level planner.

Environment	Dataset	CEM	π_{prior}	CEM + π_{prior}	Dijkstra + CEM	Dijkstra + π_{prior}	ALPS
pointmaze	pointmaze-medium-navigate-v0	58 \pm 8	19 \pm 8	30 \pm 7	100 \pm 0	46 \pm 10	82 \pm 10
	pointmaze-large-navigate-v0	19 \pm 11	17 \pm 10	21 \pm 9	100 \pm 0	43 \pm 10	76 \pm 7
	pointmaze-medium-stitch-v0	40 \pm 13	40 \pm 12	46 \pm 11	99 \pm 3	82 \pm 10	90 \pm 7
	pointmaze-large-stitch-v0	0 \pm 0	12 \pm 9	9 \pm 9	100 \pm 1	93 \pm 4	96 \pm 2
antmaze	antmaze-medium-navigate-v0	0 \pm 0	50 \pm 10	57 \pm 8	0 \pm 0	92 \pm 5	95 \pm 4
	antmaze-large-navigate-v0	0 \pm 0	30 \pm 11	29 \pm 12	0 \pm 0	90 \pm 4	94 \pm 3
	antmaze-medium-stitch-v0	0 \pm 0	50 \pm 13	55 \pm 12	0 \pm 0	92 \pm 4	95 \pm 4
	antmaze-large-stitch-v0	0 \pm 0	14 \pm 8	11 \pm 7	0 \pm 0	93 \pm 2	95 \pm 2
	antmaze-medium-explore-v0	0 \pm 0	11 \pm 6	7 \pm 3	47 \pm 22	92 \pm 4	100 \pm 0
	antmaze-large-explore-v0	0 \pm 0	1 \pm 1	0 \pm 0	11 \pm 8	43 \pm 9	91 \pm 13
humanoidmaze	humanoidmaze-medium-navigate-v0	0 \pm 0	29 \pm 12	26 \pm 10	0 \pm 0	86 \pm 6	86 \pm 6
	humanoidmaze-large-navigate-v0	0 \pm 0	3 \pm 2	3 \pm 2	0 \pm 0	58 \pm 6	54 \pm 5
	humanoidmaze-medium-stitch-v0	0 \pm 0	33 \pm 8	31 \pm 7	0 \pm 0	64 \pm 6	62 \pm 6
	humanoidmaze-large-stitch-v0	0 \pm 0	2 \pm 2	1 \pm 2	0 \pm 0	37 \pm 5	35 \pm 5

for further details. Importantly, our results are particularly significant because all the GCRL baselines we considered are model-free methods, due to the historical difficulty of getting model-based methods to succeed in these tasks. Furthermore, note that ALPS is more robust to the size of the maze the agent navigates, handily outperforming model-free baselines in the giant mazes. This result provides evidence that the Laplacian representation could be a useful building block for successful planning with a learned model, the central hypothesis of this paper.

Two sets of results are particularly interesting to discuss here. First, ALPS’s performance is closer to the baseline on the *pointmaze-navigate* tasks. These are the simplest tasks in OGBench, and here the behavior prior hinders performance. When this prior is removed, ALPS achieves a success rate close to 100% in the medium and large mazes, as shown in the ablation study in the next section. This is not surprising, as the introduced inductive bias is intended to help in substantially harder tasks.

The *teleport* mazes are also particularly interesting in the context of the Laplacian representation. When an agent enters a teleporter, it may reappear elsewhere in the maze or in an inescapable absorbing region from which the goal cannot be reached. Despite ALPS’s strong overall performance in these environments, inspection reveals it would be unable to achieve a 100% success rate. This limitation arises from the symmetries enforced by the ALLO objective: the learned Laplacian representation embeds teleporter entrances and exits as nearby states, incentivizing the agent to use the teleporter, which is suboptimal due to the risk of entering an inescapable region. To the best of our knowledge, these results are the first to suggest that the symmetrization function commonly used when learning Laplacian representations can be problematic, as prior work has reported success in asymmetric environments (Klissarov & Machado, 2023).

6. Ablation Studies

Results thus far demonstrate that the Laplacian representation can be used in hierarchical decision-time planning with images and in large continuous state and action spaces. This section provides additional analysis to better understand ALPS’s empirical success.

6.1. Components of ALPS

We perform a series of ablations to investigate how the components of ALPS influence the performance of the agent. Our aim is to disentangle the roles of CEM and the behavior prior in the low-level planner and to understand the contribution of the high-level planner to ALPS’ performance on the OGBench tasks. We compare ALPS with five variations, each including one or two of the following components: the high-level planner (Dijkstra+), CEM, and π_{prior} . We perform hyperparameter tuning for all ablations, reported in Table 7. A subset of results are presented in Table 3, with full results reported in Table 12. We follow the same evaluation procedure as described in Section 5.

The role of the Behavior Prior: Without the behavior prior (CEM, Dijkstra + CEM), performance dramatically reduces in locomotion tasks with challenging movement dynamics like ant and humanoid. We suspect two reasons for this observation. First, this reflects the slow convergence of CEM when only using noise to generate proposal trajectories, the original motivation for including a behavior prior. Second, we believe that random actions lead to out-of-distribution transitions for the forward model. The effect of the forward model being partially responsible due to out-of-distribution transitions can be observed in the outlier performance of the *explore* dataset, which has greater state-action space coverage.

The role of CEM: CEM is most impactful when the expert policy used to generate the dataset is not ideal. This is

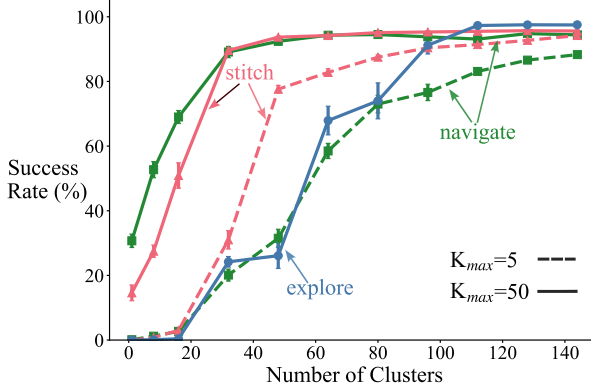


Figure 3. Success rate vs. number of clusters on OGBench *large* maze for *ant* task and types (*navigate*, *stitch*, *explore*). Error bars indicate standard error.

supported by the reduced performance of Dijkstra + π_{prior} in the *explore* datasets as compared to ALPS. More surprising is the favorable performance of Dijkstra + CEM over Dijkstra + π_{prior} in the pointmaze task with the *navigate* dataset. We believe this is primarily due to the structure of the *navigate* dataset. Because the agent visits multiple goals in sequence within a single trajectory, the dataset contains both approaching and departing behaviors with respect to each goal. As a result, the behavior prior may learn a stationary policy in regions near the goal. We observed this behavior in these settings when investigating this performance.

The role of Hierarchical Planning: The low-level planner alone is unable to effectively reach the goal in these environments, as seen by the drop in performance across the CEM, π_{prior} , and CEM + π_{prior} variants. When the hierarchical planner is added back (denoted by “Dijkstra+”) the results generally improve across domains, and especially in domains with noisy data-generating policies (e.g., *explore* datasets). The relationship between the high-level planner and the quality of the low-level planner is expanded on below. This result clearly demonstrates the importance of hierarchical planning for long-horizon planning in ALPS.

6.2. Number of Clusters

We investigate how the performance of ALPS is impacted by the number of clusters used by the high-level planner and the effective planning horizon of the behavior prior, i.e., the state-to-subgoal distance at which the behavior prior can produce good plans. The results, reported in Figure 3, reveal why ALPS is so dominant on the *explore* datasets. As the effective horizon of the data generation policy reduces, i.e., when we artificially reduce K_{max} or when the expert-data quality is reduced as in the *explore* dataset, we can simply increase the number of partitions in our high-level planner to overcome the limitation of the low-level planner. In other words, ALPS is robust to the quality of the process used to generate the expert dataset, unlike the baselines.

7. Related Work

Several methods have been proposed to solve the GCRL problem setting. A common strategy to solve this problem is to include the goal as input to a value function or policy (Schaul et al., 2015; Nair et al., 2018; Chane-Sane et al., 2021), but this approach often struggles as the time horizon increases (Nachum et al., 2018; Levy et al., 2019). Hierarchical approaches decompose the problem into manageable subproblems, alleviating many of the issues of a flat approach. Hierarchical planning can be done model-free by learning a high- and low-level policy (Levy et al., 2019; Park et al., 2023), or, like ALPS, model-based using MPC for long-term reasoning (Nasiriany et al., 2019; Nair & Finn, 2020; Pertsch et al., 2021).

Although hierarchical strategies have shown considerable promise for long-horizon problems, a common challenge is identifying subgoals. Graph partitioning has been widely used to create abstractions of the state space by identifying bottleneck states in the transition graph (McGovern & Barto, 2001; Menache et al., 2002; Şimşek et al., 2005). Similarly to ALPS and PCLast, HILP (Park et al., 2024b) uses Hilbert representation to approximate temporal distances. However, the smoothness induced by the Hilbert representation obscures natural boundaries, making partitioning difficult. Furthermore, several approaches have instead developed generative models for subgoal generation (Nair et al., 2018; Chane-Sane et al., 2021).

8. Conclusion

In this paper, we demonstrate the utility of the Laplacian representation for decision-time planning through the development and evaluation of ALPS. ALPS is able to successfully plan in continuous high-dimensional state spaces from pre-collected datasets. Furthermore, we show that hierarchical planning is necessary for ALPS’ success in these domains, especially when the example trajectories are not ideal, through ablation studies. Finally, we show that a model-based approach can outperform model-free baselines in domains like OGBench, where model-based baselines have historically performed poorly.

There are several promising directions for advancing the application of the Laplacian representation in model-based planning. In Section 6, we demonstrate that a lower-quality low-level planner can be overcome by increasing the number of subgoals used in the high-level planner. Developing a better low-level planner to use with the Laplacian representation could unlock planning at even longer horizons. Another avenue for future work is to investigate stacking the Laplacian representation on-top of a lower level latent space. Similarly to PCLast, which uses ACRO, an intermediate representation could improve the performance of ALPS.

Impact Statement

This paper presents work whose goal is to advance the field of Machine Learning. There are many potential societal consequences of our work, none which we feel must be specifically highlighted here.

Acknowledgements

We thank Diego Gomez for providing an initial version of the ALLO objective and Siddarth Chandersekhar, along with members of the Reinforcement Learning and Artificial Intelligence (RLAI) lab, for helpful discussions and feedback. This research was supported in part by the Natural Sciences and Engineering Research Council of Canada (NSERC), Alberta Machine Intelligence Institute (Amii), Canada CIFAR AI Chair Program, Mitacs, and Alberta Innovates. It was also enabled in part by computational resources provided by the Digital Research Alliance of Canada.

References

Bharadhwaj, H., Xie, K., and Shkurti, F. Model-predictive control via cross-entropy and gradient-based optimization. In *Learning for Dynamics and Control (L4DC)*, 2020.

Chane-Sane, E., Schmid, C., and Laptev, I. Goal-conditioned reinforcement learning with imagined subgoals. In *International Conference on Machine Learning (ICML)*, 2021.

Chua, K., Calandra, R., McAllister, R., and Levine, S. Deep reinforcement learning in a handful of trials using probabilistic dynamics models. *Neural Information Processing Systems (NeurIPS)*, 2018.

Clavera, I., Rothfuss, J., Schulman, J., Fujita, Y., Asfour, T., and Abbeel, P. Model-based reinforcement learning via meta-policy optimization. In *Conference on robot learning (CoRL)*, 2018.

Şimşek, O., Wolfe, A. P., and Barto, A. G. Identifying useful subgoals in reinforcement learning by local graph partitioning. In *International Conference on Machine Learning (ICML)*, 2005.

Deisenroth, M. P. and Rasmussen, C. E. PILCO: A model-based and data-efficient approach to policy search. In *International Conference on Machine Learning (ICML)*, 2011.

Dijkstra, E. W. A note on two problems in connexion with graphs. *Numerische Mathematik*, 1959.

Eysenbach, B., Zhang, T., Levine, S., and Salakhutdinov, R. R. Contrastive learning as goal-conditioned reinforcement learning. *Neural Information Processing Systems (NeurIPS)*, 2022.

Feinberg, V., Wan, A., Stoica, I., Jordan, M. I., Gonzalez, J. E., and Levine, S. Model-based value estimation for efficient model-free reinforcement learning. *International Conference on Machine Learning (ICML)*, 2018.

Finn, C. and Levine, S. Deep visual foresight for planning robot motion. In *IEEE International Conference on Robotics and Automation (ICRA)*, 2017.

García, C. E., Prett, D. M., and Morari, M. Model predictive control: Theory and practice—a survey. *Automatica*, 25 (3):335–348, 1989.

Ghosh, D., Gupta, A., Reddy, A., Fu, J., Devin, C. M., Eysenbach, B., and Levine, S. Learning to reach goals via iterated supervised learning. In *International Conference on Learning Representations (ICLR)*, 2021.

Gomez, D., Bowling, M., and Machado, M. C. Proper Laplacian representation learning. In *International Conference on Learning Representations (ICLR)*, 2023.

Gu, S., Lillicrap, T., Sutskever, I., and Levine, S. Continuous deep Q-learning with model-based acceleration. In *International Conference on Machine Learning (ICML)*, 2016.

Gürtler, N. and Martius, G. Long-horizon planning with predictable skills. *Reinforcement Learning Journal (RLJ)*, 2025.

Haarnoja, T., Zhou, A., Abbeel, P., and Levine, S. Soft actor-critic: Off-policy maximum entropy deep reinforcement learning with a stochastic actor. In *International Conference on Machine Learning (ICML)*, 2018.

Hafner, D., Lillicrap, T., Fischer, I., Villegas, R., Ha, D., Lee, H., and Davidson, J. Learning latent dynamics for planning from pixels. In *International Conference on Machine Learning (ICML)*, 2019.

Hansen, N., Su, H., and Wang, X. TD-MPC2: Scalable, robust world models for continuous control. In *International Conference on Learning Representations (ICLR)*, 2024.

Holtzman, A., Buys, J., Du, L., Forbes, M., and Choi, Y. The curious case of neural text degeneration. In *International Conference on Learning Representations (ICLR)*, 2020.

Islam, R., Tomar, M., Lamb, A., Efroni, Y., Zang, H., Didolkar, A., Misra, D., Li, X., Van Seijen, H., Combes, R. T. d., and Langford, J. Agent-controller representations: Principled offline RL with rich exogenous information. In *International Conference on Machine Learning (ICML)*, 2023.

Janner, M., Fu, J., Zhang, M., and Levine, S. When to trust your model: Model-based policy optimization. *Neural Information Processing Systems (NeurIPS)*, 2019.

Jinnai, Y., Abel, D., Hershkowitz, D., Littman, M., and Konidaris, G. Finding options that minimize planning time. In *International Conference on Machine Learning (ICML)*, 2019.

Jinnai, Y., Park, J. W., Machado, M. C., and Konidaris, G. Exploration in reinforcement learning with deep covering options. In *International Conference on Learning Representations (ICLR)*, 2020.

Kaelbling, L. P. Learning to achieve goals. In *International Joint Conference on Artificial Intelligence (IJCAI)*, 1993.

Kingma, D. P. Adam: A method for stochastic optimization. *International Conference on Learning Representations (ICLR)*, 2015.

Klein, D. and Randić, M. Resistance distance. *Journal of Mathematical Chemistry (JOMC)*, 1993.

Klissarov, M. and Machado, M. C. Deep Laplacian-based options for temporally-extended exploration. In *International Conference on Machine Learning (ICML)*, 2023.

Kocsis, L. and Szepesvári, C. Bandit based Monte-Carlo planning. In *European Conference on Machine Learning (ECML)*, 2006.

Kostrikov, I., Nair, A., and Levine, S. Offline reinforcement learning with Implicit Q-Learning. In *International Conference on Learning Representations (ICLR)*, 2022.

Koul, A., Sujit, S., Chen, S., Evans, B., Wu, L., Xu, B., Chari, R., Islam, R., Seraj, R., Efroni, Y., Molu, L., Dudik, M., Langford, J., and Lamb, A. PcLast: Discovering plannable continuous latent states. In *International Conference on Machine Learning (ICML)*, 2024.

Lambert, N., Pister, K., and Calandra, R. Investigating compounding prediction errors in learned dynamics models. *arXiv preprint arXiv:2203.09637*, 2022.

Levy, A., Konidaris, G., Platt, R., and Saenko, K. Hierarchical reinforcement learning with hindsight. In *International Conference on Learning Representations (ICLR)*, 2019.

Liu, M., Zhu, M., and Zhang, W. Goal-conditioned reinforcement learning: Problems and solutions. *International Joint Conference on Artificial Intelligence (IJCAI)*, 2022.

Lovász, L., Winkler, P., Lukács, A., and Kotlov, A. Random walks on graphs: A survey. In *Combinatorics, Paul Erdős is eighty*, 1993.

Lynch, C., Khansari, M., Xiao, T., Kumar, V., Tompson, J., Levine, S., and Sermanet, P. Learning latent plans from play. In *Conference on Robot Learning (CoRL)*, 2020.

Machado, M. C., Bellemare, M. G., and Bowling, M. A Laplacian framework for option discovery in reinforcement learning. In *International Conference on Machine Learning (ICML)*, 2017.

Machado, M. C., Barreto, A., Precup, D., and Bowling, M. Temporal abstraction in reinforcement learning with the successor representation. *Journal of Machine Learning Research (JMLR)*, 2023.

Mahadevan, S. Proto-value functions: developmental reinforcement learning. *International Conference on Machine Learning (ICML)*, 2005.

Mahadevan, S. and Maggioni, M. Proto-value functions: A Laplacian framework for learning representation and control in Markov Decision Processes. *Journal of Machine Learning Research (JMLR)*, 2007.

McGovern, A. and Barto, A. G. Automatic discovery of sub-goals in reinforcement learning using diverse density. In *International Conference on Machine Learning (ICML)*, 2001.

Menache, I., Mannor, S., and Shimkin, N. Q-cut—dynamic discovery of sub-goals in reinforcement learning. In *European Conference on Machine Learning (ECML)*, 2002.

Nachum, O., Gu, S. S., Lee, H., and Levine, S. Data-efficient hierarchical reinforcement learning. *Neural Information Processing Systems (NeurIPS)*, 2018.

Nair, A. V., Pong, V., Dalal, M., Bahl, S., Lin, S., and Levine, S. Visual reinforcement learning with imagined goals. *Neural Information Processing Systems (NeurIPS)*, 2018.

Nair, S. and Finn, C. Hierarchical foresight: Self-supervised learning of long-horizon tasks via visual subgoal generation. *International Conference on Learning Representations (ICLR)*, 2020.

Nasiriany, S., Pong, V., Lin, S., and Levine, S. Planning with goal-conditioned policies. *Neural Information Processing Systems (NeurIPS)*, 2019.

Ng, A., Jordan, M., and Weiss, Y. On spectral clustering: Analysis and an algorithm. *Neural Information Processing Systems (NeurIPS)*, 2001.

Park, S., Ghosh, D., Eysenbach, B., and Levine, S. HIQL: Offline goal-conditioned RL with latent states as actions. *Neural Information Processing Systems (NeurIPS)*, 2023.

Park, S., Frans, K., Levine, S., and Kumar, A. Is value learning really the main bottleneck in offline RL? *Neural Information Processing Systems (NeurIPS)*, 2024a.

Park, S., Kreiman, T., and Levine, S. Foundation policies with hilbert representations. In *International Conference on Machine Learning (ICML)*, 2024b.

Park, S., Frans, K., Eysenbach, B., and Levine, S. OG-Bench: Benchmarking offline goal-conditioned RL. In *International Conference on Learning Representations (ICLR)*, 2025.

Pertsch, K., Lee, Y., and Lim, J. Accelerating reinforcement learning with learned skill priors. In *Conference on Robot Learning (CoRL)*, 2021.

Pinneri, C., Sawant, S., Blaes, S., Achterhold, J., Stueckler, J., Rolinek, M., and Martius, G. Sample-efficient cross-entropy method for real-time planning. In *Conference on Robot Learning (CoRL)*, 2021.

Qiu, H. and Hancock, E. R. Clustering and embedding using commute times. *IEEE Pattern Analysis and Machine Intelligence (TPAMI)*, 2007.

Rubinstein, R. Y. Optimization of computer simulation models with rare events. *European Journal of Operational Research (EJOR)*, 1997.

Schaul, T., Horgan, D., Gregor, K., and Silver, D. Universal value function approximators. In *International Conference on Machine Learning (ICML)*, 2015.

Shi, J. and Malik, J. Normalized cuts and image segmentation. *IEEE Pattern Analysis and Machine Intelligence (TPAMI)*, 2000.

Sutton, R. S. Dyna, an integrated architecture for learning, planning, and reacting. *ACM SIGART Bulletin*, 2(4): 160–163, 1991.

Talvitie, E. Model regularization for stable sample rollouts. In *Uncertainty in Artificial Intelligence (UAI)*, 2014.

Talvitie, E. Self-correcting models for model-based reinforcement learning. In *Association for the Advancement of Artificial Intelligence (AAAI)*, 2017.

Venkatraman, A., Hebert, M., and Bagnell, J. A. Improving multi-step prediction of learned time series models. In *Association for the Advancement of Artificial Intelligence (AAAI)*, 2015.

Von Luxburg, U. A tutorial on spectral clustering. *Statistics and Computing*, 2007.

Wan, Y., Rahimi-Kalhroudi, A., Rajendran, J., Momennejad, I., Chandar, S., and Van Seijen, H. H. Towards evaluating adaptivity of model-based reinforcement learning methods. In *International Conference on Machine Learning (ICML)*, 2022.

Wang, K., Zhou, K., Zhang, Q., Shao, J., Hooi, B., and Feng, J. Towards better laplacian representation in reinforcement learning with generalized graph drawing. In *International Conference on Machine Learning (ICML)*, 2021.

Wang, K., Zhou, K., Feng, J., Hooi, B., and Wang, X. Reachability-aware Laplacian representation in reinforcement learning. In *International Conference on Machine Learning (ICML)*, 2023a.

Wang, T. and Ba, J. Exploring model-based planning with policy networks. *International Conference on Learning Representations (ICLR)*, 2020.

Wang, T., Bao, X., Clavera, I., Hoang, J., Wen, Y., Langlois, E., Zhang, S., Zhang, G., Abbeel, P., and Ba, J. Benchmarking model-based reinforcement learning. *arXiv preprint arXiv:1907.02057*, 2019.

Wang, T., Torralba, A., Isola, P., and Zhang, A. Optimal goal-reaching reinforcement learning via quasimetric learning. In *International Conference on Machine Learning (ICML)*, 2023b.

Weiss, Y. Segmentation using eigenvectors: a unifying view. In *IEEE International Conference on Computer Vision (ICCV)*, 1999.

Werbos, P. Backpropagation through time: what it does and how to do it. *Proceedings of the IEEE*, 1990.

Wu, Y., Tucker, G., and Nachum, O. The Laplacian in rl: Learning representations with efficient approximations. In *International Conference on Learning Representations (ICLR)*, 2019.

Xiao, W. and Gutman, I. Resistance distance and Laplacian spectrum. *Theoretical Chemistry Accounts*, 2003.

Yu, T., Thomas, G., Yu, L., Ermon, S., Zou, J. Y., Levine, S., Finn, C., and Ma, T. MOPO: Model-based offline policy optimization. *Neural Information Processing Systems (NeurIPS)*, 2020.

Zhang, J., Cheung, B., Finn, C., Levine, S., and Jayaraman, D. Cautious adaptation for reinforcement learning in safety-critical settings. In *International Conference on Machine Learning (ICML)*, 2020.

A. Further Background

In this section, we provide further mathematical details for completeness.

A.1. CTD

For completeness, we include the transformation of CTD to the scaled Laplacian representation following from (Lovász et al., 1993) and (Klein & Randić, 1993). CTD, $c(u, v)$ is defined as the expected number of steps it takes to travel from node u to v and back to u from a random walk (Lovász et al., 1993). If we divide the Laplacian eigenvector by the square root of its corresponding eigenvalue, this scaled Laplacian representation approximates the CTD. We can compute the CTD on a graph using the generalized inverse \mathbf{L}^\dagger of the graph Laplacian \mathbf{L} (Klein & Randić, 1993). Since, \mathbf{L} is eigendecomposable, $\mathbf{L}^\dagger = \sum_{i=1}^{n-1} \frac{1}{\lambda_i} \mathbf{u}_i \mathbf{u}_i^\top$. Specifically for computing the commute time, we have:

$$c(u, v) = \text{vol}(\mathcal{G})(l_{uu}^\dagger - 2l_{uv}^\dagger + l_{vv}^\dagger) \quad (5)$$

where $\text{vol}(\mathcal{G}) = \sum_{u \in \mathcal{S}} d(u)$ is the volume of the graph, which is constant for a static graph, and $\mathbf{L}^\dagger = (l_{uv}^\dagger)_{u, v=1, \dots, n}$. We can plug \mathbf{L}^\dagger into Eq. 5:

$$\begin{aligned} l_{uu}^\dagger - 2l_{uv}^\dagger + l_{vv}^\dagger &= \sum_{i=1}^{n-1} \frac{1}{\lambda_i} \mathbf{u}_i(u)^2 - 2 \sum_{i=1}^{n-1} \frac{1}{\lambda_i} \mathbf{u}_i(u) \mathbf{u}_i(v) + \sum_{i=1}^{n-1} \frac{1}{\lambda_i} \mathbf{u}_i(v)^2 \\ &= \sum_{i=1}^{n-1} \frac{1}{\lambda_i} \left(\mathbf{u}_i(u)^2 - 2\mathbf{u}_i(u) \mathbf{u}_i(v) + \mathbf{u}_i(v)^2 \right) \\ &= \sum_{i=1}^{n-1} \frac{1}{\lambda_i} \left(\mathbf{u}_i(u) - \mathbf{u}_i(v) \right)^2 \\ &= \sum_{i=1}^{n-1} \left(\frac{\mathbf{u}_i(u)}{\sqrt{\lambda_i}} - \frac{\mathbf{u}_i(v)}{\sqrt{\lambda_i}} \right)^2 \end{aligned} \quad (6)$$

Therefore, we define this scaled Laplacian representation Ψ as :

$$\Psi(u) = \left(\frac{\mathbf{u}_1(u)}{\sqrt{\lambda_1}}, \frac{\mathbf{u}_2(u)}{\sqrt{\lambda_2}}, \dots, \frac{\mathbf{u}_{n-1}(u)}{\sqrt{\lambda_{n-1}}} \right)^\top \quad (7)$$

The Euclidean distance in this Ψ space is directly proportional to the commute distance in the original space:

$$c_{uv} \propto \sum_{i=1}^{n-1} \left(\frac{\mathbf{u}_i(u)}{\sqrt{\lambda_i}} - \frac{\mathbf{u}_i(v)}{\sqrt{\lambda_i}} \right)^2 \quad (8)$$

B. Baselines

We briefly explain all the baselines considered in this section.

B.1. PcLast

Plannable Continuous Latent States (PcLast; Koul et al., 2024) maps observations to a latent representation and associates neighboring states together by optimizing a contrastive loss:

$$\begin{aligned} \arg \min_{\Gamma, \alpha, \beta} & - \left(\log \left(\sigma(e^\alpha - e^\beta \|\Gamma(\xi(s_t)) - \Gamma(\xi(s_{t+d}))\|^2) \right) \right. \\ & \left. + \log \left(1 - \sigma(e^\alpha - e^\beta \|\Gamma(\xi(s_t)) - \Gamma(\xi(s_r))\|^2) \right) \right) \end{aligned} \quad (9)$$

where ξ is a space representation to remove exogenous noise (Islam et al., 2023), Γ is the PcLast space, s_t and s_{t+d} are positive pairs d transitions apart, with s_r as a negative example, sampled uniformly from the data buffer, α and β are the hyperparameters.

B.2. OGBench Baselines

- **Goal-Conditioned Behavior Cloning** (Lynch et al., 2020; Ghosh et al., 2021) is a baseline that performs behavior cloning by sampling a future state from the same trajectory as the goal.
- **Goal-Conditioned Implicit {V, Q}-Learning** are goal-conditioned variants of implicit Q-Learning (IQL; Kostrikov et al., 2022) that fits optimal value functions (V^* and Q^*) using expectile regression.
- **Quasimetric RL** (Wang et al., 2023b) learns a quasimetric distance function that satisfies the triangle inequality and uses this to represent goal-conditioned value functions.
- **Contrastive RL** (Eysenbach et al., 2022) uses contrastive learning to learn a goal-conditioned value function.
- **Hierarchical Implicit Q-Learning** (Park et al., 2023) is a hierarchical model-free algorithm where the high-level predicts the representation of an optimal k -step subgoal, and the low-level policy predicts the optimal action for this subgoal.

C. Cross-Entropy Method for Decision-time Planning

The Cross-Entropy Method (CEM; Rubinstein, 1997) is a popular MPC-based planner that has been successful in model-based RL settings (Finn & Levine, 2017; Chua et al., 2018; Hafner et al., 2019; Pinneri et al., 2021; Gürtler & Martius, 2025). CEM begins by sampling action sequences from a normal distribution and updating its mean and variance based on the lowest-cost trajectories. We used the behavior prior, π_{prior} , to generate the initial action sequence. π_{prior} predicts an action \hat{A}_t in a state S_t , which is then fed to the forward model f to predict the next state \hat{S}_{t+1} . This predicted state \hat{S}_{t+1} is then fed back to π_{prior} to predict \hat{A}_{t+1} . This process repeats until the planning horizon H , resulting in an action sequence $\mathbf{a}_{t:t+H-1}$. Correlated noise is then added to the initial action sequence to generate multiple action sequences. CEM uses these action sequences to generate multiple trajectories, whose costs are computed in scaled Laplacian representation, ψ -space, because it is isometric to CTD. The CEM algorithm is outlined in Algorithm 2.

Algorithm 2 Cross-Entropy Method Planner

```

Input:  $s, z_{\text{sub}}, \psi, f, \pi_{\text{prior}}$ 
CEM parameters: planner horizon  $H$ , iterations  $N_{\text{iter}}$ , number of samples  $N_s$ , elite ratio  $N_e$ 
==== Warm Start CEM with Policy ====
 $\mathbf{a}_{1:H} \leftarrow \text{rollout } \pi_{\text{prior}} \text{ from } s$ 
==== CEM iterations ====
for  $i = 1$  to  $N_{\text{iter}}$  do
    sample  $\{\mathbf{a}_{1:H}^j\}_{j=1}^{N_s}$  around  $\mathbf{a}_{1:H}$  ▷ sample action sequences
    === Cost Computation ===
    for  $j = 1$  to  $N_s$  do
         $\{\hat{S}_t\}_{t=1}^H \leftarrow f(s, \mathbf{a}_{1:H}^j)$  ▷ rollout action sequences using  $f$ 
         $J^j \leftarrow \sum_{t=1}^H (\|\psi(\hat{S}_t^j) - z_{\text{sub}}\| + \lambda \|\mathbf{a}_t^j\|^2)$ 
    end for
     $\mathbf{a}_{1:H} \leftarrow \text{mean of top-}N_e \text{ elite trajectories}$  ▷ update sampling distribution
end for
return  $\mathbf{a}_{1:H}$ 

```

D. Environments

In this section, we will discuss all the environments that were considered for evaluation of ALPS.

D.1. Maze2D—PointMass Environments

We introduce the *Maze2D—PointMass* environments here, originally discussed in (Koul et al., 2024). These environments are 2D maze point-mass environments with continuous states and actions. The environments have varied wall configurations, with the goal of reaching in vicinity of a desired position. The agent controls a point mass with actions corresponding to the coordinate space change $(\Delta x, \Delta y)$ bounded by the range $[-0.2, 0.2]$ for each action. Observations are defined as a single-channel (100×100) image encoding the current position of the agent and no other environmental information. A

Gaussian blur ($\sigma = 1.0$) is applied to the agent's coordinate position, and the resulting image is normalized to $[0, 1]$ (Fig. 4d). In the presence of obstacles, the point mass starts from s_t and is moved along the direction of a_t until it collides with an obstacle. An episode lasts for 30 time steps, and it terminates if the agent reaches within 0.03 units of the goal. We consider three variants: *Hallway*, *Rooms*, and *Spiral* of the Maze environment, whose layouts are shown in Fig. 4.

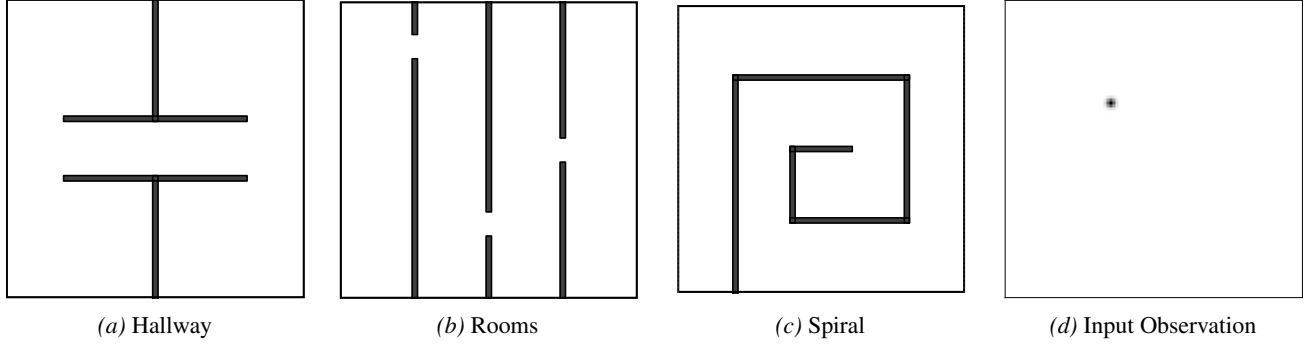


Figure 4. (a)-(c) 2-D Maze environments with continuous state and action spaces, (d) Input observation

D.2. OGBench Environments

Here, we lay out all the mazes considered in the OGBench for locomotion tasks. It consists of four mazes: *medium*, *large*, *giant*, and *teleport* (Fig. 5). *giant* maze is the largest maze, twice the size of *large*, and is primarily designed to test the agent's long-horizon reasoning. *teleport* is a stochastic environment with teleportation gates: black hole as teleport-in and white hole as teleport-out. If the agent enters the black hole, it is randomly spawned at any of the white holes. One of the white holes is a dead end; thus, accessing the teleport holes is risky. Hence, the agent must learn to avoid black holes to complete the task reliably.

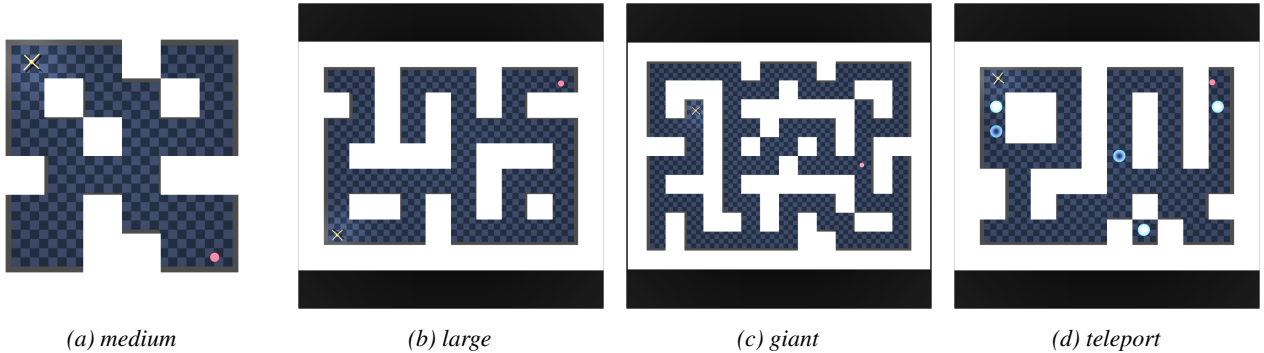


Figure 5. OGBench Mazes

We consider the following locomotion tasks: (1) *pointmaze*, which involves controlling a 2-DoF point mass, (2) *antmaze*, which involves controlling an 8-DoF quadruped ant, and (3) *humanoidmaze*, which involves controlling a 21-DoF humanoid. The agent is required to reach a desired location in the environment in these locomotion tasks.

There are three dataset variants, each collected through a directional policy trained via SAC (Haarnoja et al., 2018) and a high-level waypoint controller. The dataset types are as follows: (i) *navigate*, collected by a noisy expert policy that navigates the maze by repeatedly reaching randomly sampled goals, (ii) *stitch*, collected through shorter goal-reaching trajectories from a noisy expert, which test the agent's stitching ability, and (iii) *explore*, collected by commanding the low-level policy with a large amount of action noise, aimed to test agent's navigation skills from an extremely low-quality (yet high-coverage) data.

The agent has to learn both mapping skills to navigate and locomotion skills to control the agent. An episode is terminated as soon as the agent reaches within the proximity of the goal location, which is 0.5 units for *pointmaze* and 1 unit for *antmaze/humanoidmaze*, defining the success, or the episode end is reached, which varies for different environments.

Table 4. Environment specifications

Environment Type	Environment	State Dimension	Action Dimension	Maximum Episode Length
pointmaze	pointmaze-medium-v0	2	2	1000
	pointmaze-large-v0	2	2	1000
	pointmaze-giant-v0	2	2	1000
	pointmaze-teleport-v0	2	2	1000
antmaze	antmaze-medium-v0	29	8	1000
	antmaze-large-v0	29	8	1000
	antmaze-giant-v0	29	8	1000
	antmaze-teleport-v0	29	8	1000
humanoidmaze	humanoidmaze-medium-v0	69	21	2000
	humanoidmaze-large-v0	69	21	2000
	humanoidmaze-giant-v0	69	21	4000

Table 5. Dataset specifications

Environment Type	Dataset Type	Dataset	# Transitions	# Episodes	Data Episode Length
pointmaze	navigate	pointmaze-medium-navigate-v0	1M	1000	1000
		pointmaze-large-navigate-v0	1M	1000	1000
		pointmaze-giant-navigate-v0	1M	500	2000
		pointmaze-teleport-navigate-v0	1M	1000	1000
	stitch	pointmaze-medium-stitch-v0	1M	5000	200
		pointmaze-large-stitch-v0	1M	5000	200
		pointmaze-giant-stitch-v0	1M	5000	200
		pointmaze-teleport-stitch-v0	1M	5000	200
antmaze	navigate	antmaze-medium-navigate-v0	1M	1000	1000
		antmaze-large-navigate-v0	1M	1000	1000
		antmaze-giant-navigate-v0	1M	500	2000
		antmaze-teleport-navigate-v0	1M	1000	1000
	stitch	antmaze-medium-stitch-v0	1M	5000	200
		antmaze-large-stitch-v0	1M	5000	200
		antmaze-giant-stitch-v0	1M	5000	200
		antmaze-teleport-stitch-v0	1M	5000	200
humanoidmaze	explore	antmaze-medium-explore-v0	5M	10000	500
		antmaze-large-explore-v0	5M	10000	500
		antmaze-teleport-explore-v0	5M	10000	500
	navigate	humanoidmaze-medium-navigate-v0	2M	1000	2000
		humanoidmaze-large-navigate-v0	2M	1000	2000
		humanoidmaze-giant-navigate-v0	4M	1000	4000
	stitch	humanoidmaze-medium-stitch-v0	2M	5000	400
		humanoidmaze-large-stitch-v0	2M	5000	400
		humanoidmaze-giant-stitch-v0	4M	10000	400

Since the number of environmental steps and the dataset collection procedure differ across environments, we report both the environment and dataset specifications in Table 4 and Table 5, respectively.

Each task in OGBench has 5 pre-defined start-goal pairs, which are slightly randomized on every reset. Thus, following the protocols of OGBench, we evaluate the performance using 250 episodes per checkpoints (50 rollouts for each of the 5 pairs). Since ALPS involves sequential training, we adopt a stated evaluation protocol. The Laplacian representation from ALLO is first pre-trained and frozen at three distinct checkpoints (800K, 900K, and 1M) steps. Then, behavior is trained with these weights for the corresponding time steps. The final performance is averaged across these three evaluation stages and 8 random seeds to ensure statistical robustness.

E. Experimental Setup

E.1. Statistical Testing

Results reported in Section 5 on OGBench are statistically tested using the Wilcoxon signed-rank test. For each baseline, ALPS and the baseline are compared across datasets to show the two algorithms aren't drawing from the same distribution. Because we are testing across multiple baselines with a single sample of ALPS we use the Holm-Bonferroni corrections. We set an acceptable error rate of $p < 0.01$, which our tests show was too cautious in Table 6.

Table 6. Wilcoxon signed-rank test p -values (two-sided) with Holm-Bonferroni correction comparing ALPS against baselines.

	GCBC	GCIVL	GCIQL	QRL	CRL	HIQL
p -value	0.000001	0.000017	0.000001	0.000077	0.000070	0.000556

E.2. Architecture

We use the same architecture for all domains. The ALLO encoder ϕ is a four-layer MLP network with hidden layers of size 256. The first layer has Layer norm followed by a tanh activation, while all other layers have ReLU activation. The network outputs 32 eigenvectors, decided by a sweep over 16, 32, and 64. The forward model f network is a four-layer MLP with hidden layers of size 512 and ReLU activations. The behavior prior π_{prior} is a four-layer MLP with hidden size 512 and ReLU activations. For image states, three convolutional layers are prepended to all networks.

For training the ALLO encoder, we set the geometric distribution parameter $\gamma_s = 0.2$ for PcLast environments and $\gamma_s = 0.6$ for OG Bench. All other hyperparameters are default from [Gomez et al. \(2023\)](#) and listed in Table 7. These values are chosen through a sweep over values in the range $[0.2, 0.8]$. We sample pairs from the same episode, as we observed that eigenvalues are more stable with that. Unless otherwise specified, the horizon used for the behavior prior is $k \sim U[1, 50]$, and the max horizon for the forward model $H_f = 10$. All networks are trained using Adam optimizer ([Kingma, 2015](#)) with a step size of $\alpha = 10^{-4}$ for ϕ chosen as the default from ([Gomez et al., 2023](#)) and $\alpha = 3 \times 10^{-4}$ for f and π_{prior} with a batch size of 1024. We only tuned the depth of the neural networks. For domains with continuous states, we centralize the values to have zero mean and unit standard deviation. For image domains, we normalize the values to be in the range $[0, 1]$.

Table 7. Hyperparameters

Hyperparameter	Value
<i>==== ALLO Parameters ====</i>	
Sampling discount	0.6 (0.2 for <i>Maze</i>)
Number of eigenvectors	32
ALLO learning rate	1×10^{-4}
Duals initial value	-1.0
Barrier initial value	0.5
Min duals	-100.0
Max duals	100.0
Min barrier coefficients	0.0
Max barrier coefficients	0.5
Step size duals	1.0
ALLO training steps	1×10^6
<i>==== Dynamics Parameters ====</i>	
Multistep Dynamics Horizon H_f	10 (3 for <i>Maze</i>)
Dynamics learning rate	3×10^{-4}
Dynamics training steps	1×10^6
<i>==== Behavior Prior Parameters ====</i>	
Prior max horizon (K_{max})	50
Prior learning rate	3×10^{-4}
Prior training steps	1×10^6
<i>==== Planner Parameters ====</i>	
Number of clusters	64 (<i>Medium</i>), 96 (<i>Large, Teleport</i>), 128 (<i>Giant</i>)
Top- p	0.95
Noise beta (β)	0.9
Sigma (σ)	0.5
Penalty Coefficient	0.01
Planner Momentum (η)	0.3
Planner Horizon (H)	20 (2 for <i>Maze</i>)
CEM Iterations (N_{iter})	5
CEM Samples (N_s)	500
CEM Elite ratio (N_e)	0.15

The number of clusters in the cluster graph is dependent on the environment and training dataset. To construct the connections of the cluster graph, nucleus sampling with the p -value of 0.95 is chosen, inspired from [Koul et al. \(2024\)](#).

All planner parameters are consistent across all environments. The planning horizon H for the CEM is set to be 20, swept over $\{10, 20\}$. We add temporally-correlated noise with $\beta = 0.9$ and magnitude $\sigma = 0.5$ to create $N_s = 500$ trajectories around the mean trajectory rolled out from π_{prior} . The actions are refined for $N_{\text{iter}} = 5$ iterations, updating the distribution using the top $N_e = 15\%$ samples as elites. A momentum η of 0.3 is used to smooth out updates to the final mean trajectory. These values were selected by a grid search over $N_s \in \{200, 500\}$, $\sigma \in \{0.3, 0.5, 0.7\}$, $\eta \in \{0.3, 0.5, 0.7\}$. The penalty coefficient λ for penalizing large actions in the cost function is set to 0.01, selected from $\{0.01, 0.05, 0.1\}$.

F. Further Results and Visualizations

F.1. Visualization for PcLast Environments

We further show the effectiveness of the Laplacian representation using the Maze2D—PointMass Spiral environment (Fig. 4c). As shown in Fig. 6, spectral clustering correctly partitions the spiral environment into well-connected regions respecting the wall boundaries. Crucially, the learned representation captures CTD effectively. For instance, the inner part of the spiral is geometrically closer to the reference state but far in terms of temporal distance. Further, the topological accuracy provides a smooth gradient for trajectory optimization, validating ALPS’s strong performance in these Maze2D environments with only a low-level planner, as reported in Table 2.

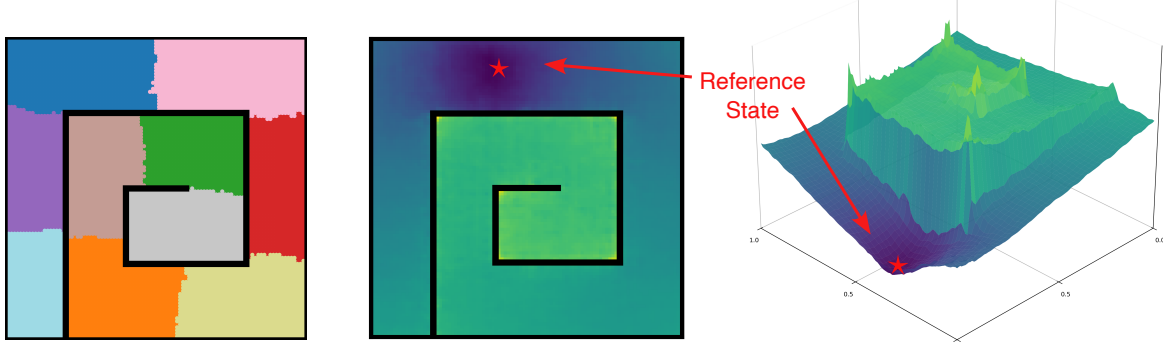


Figure 6. Visualization of the ψ -space properties in the spiral maze environment (Fig. 4c). (left) Cluster labels assigned to each state in the dataset via clustering in ψ -space. (center) Heatmap of $c(s^*, s_i)$ distance from a reference state (s^* denoted by \star in the figure) to each state in the dataset. (right) 3-D visualization of the distance landscape from the same reference state. This further validates the CTD property and spectral clustering characteristic of ψ -space.

F.2. Comparison with PcLast

In Section 5, we compared ALPS[†] and PcLast to the best of our ability using the code provided by the authors. When initially testing Plannable Continuous Latent States (PcLast) on the Maze2D-Point Mass environments without a gaussian blur, we were unable to reproduce their results. In Table 8, we report the results we were able to reproduce using their code and discussion with the authors and the original performance reported in Koul et al. (2024).

Table 8. Further results using PcLast on Maze2D-Point Mass domain. We follow the same protocol as discussed in Section 5.

Environment	Clusters	PcLast (Reported)	PcLast (Ours)
Hallway	1	88 ± 3	40 ± 2
	16	97 ± 5	69 ± 6
Rooms	1	69 ± 3	26 ± 3
	16	90 ± 10	36 ± 7
Spiral	1	50 ± 4	39 ± 4
	16	89 ± 10	60 ± 7

F.3. Teleport Environment

As discussed in the Section 5.3, *teleport* mazes pose an interesting problem in the context of the Laplacian representation. Since ALLO objective learns a symmetrized version, in ψ -space, the embeddings of teleport in and teleport out gates are close to each other. We verify this empirically in Fig. 7 where all the teleport gates are getting clustered to the same cluster. Thus, if a goal is closer to the teleport gates, the agent attempts to access them, which is suboptimal due to the risk of entering an inescapable region.

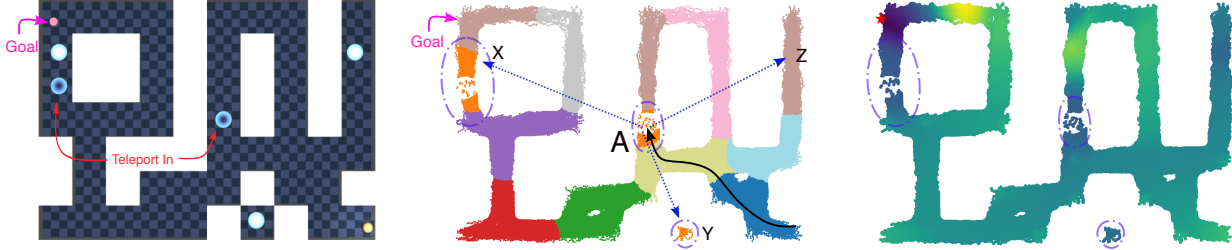


Figure 7. Visualization of the cluster assignment and Laplacian space distance for the *pointmaze-teleport* maze environment from OGBench. In this task, the goal lies closer to teleport-out gate. Since all the teleport gates are clustering together because their embeddings lies together, *ball* tries to access the teleport gate after reaching point A. However, *ball* may end up at point Y through which it cannot escape.

F.4. Individual Task Results

We report individual evaluation goals success rates for each task averaged over 150 rollouts (3 evaluation epochs \times 50 rollouts) for *pointmaze* (Table 9), *antmaze* (Table 10), and *humanoidmaze* (Table 11).

F.5. Ablations

For planning without the π_{prior} case, CEM must find optimal actions from scratch. We increase the temporally-correlated noise magnitude $\sigma = 1.0$ because CEM has to search across the entire action space. Number of CEM iterations N_{iter} is set to 15, selected from a sweep over {5, 10, 15, 20}, as CEM takes more time to converge now. The number of CEM samples N_s is also increased to 5000 as the search space is wider compared to the case when it can access the π_{prior} case, selected with a grid search over {500, 1000, 2000, 5000, 10000}. This further shows that having access to π_{prior} can accelerate the convergence of CEM with a smaller number of samples.

We report the success rates (%) of all six variants of ALPS, discussed in Section 6, in Table 12.

Table 9. Full Results on PointMaze

Environment Type	Dataset Type	Dataset	Task	GCBC	GCIVL	GCIQL	QRL	CRL	HIQL	ALPS
navigate	pointmaze-medium-navigate-v0	task1	30 ± 27	88 ± 16	97 ± 4	100 ± 0	20 ± 6	99 ± 1	69 ± 12	
		task2	3 ± 2	95 ± 10	76 ± 29	94 ± 17	45 ± 25	87 ± 7	94 ± 6	
		task3	5 ± 5	37 ± 28	10 ± 28	23 ± 20	30 ± 4	55 ± 13	75 ± 11	
		task4	0 ± 1	2 ± 2	0 ± 0	94 ± 14	28 ± 29	82 ± 12	75 ± 11	
		task5	4 ± 3	92 ± 7	79 ± 6	97 ± 8	24 ± 13	70 ± 10	94 ± 6	
	pointmaze-large-navigate-v0	overall	9 ± 6	63 ± 6	53 ± 8	82 ± 5	29 ± 7	79 ± 5	82 ± 10	
		task1	63 ± 11	76 ± 23	86 ± 14	95 ± 8	42 ± 27	83 ± 13	75 ± 11	
		task2	1 ± 2	0 ± 0	0 ± 0	100 ± 0	31 ± 24	2 ± 7	69 ± 12	
		task3	10 ± 7	98 ± 5	83 ± 8	40 ± 50	78 ± 7	88 ± 10	88 ± 9	
		task4	20 ± 18	0 ± 0	0 ± 0	96 ± 7	24 ± 14	72 ± 19	75 ± 11	
pointmaze	pointmaze-giant-navigate-v0	task5	52 ± 17	53 ± 20	0 ± 0	96 ± 7	20 ± 10	46 ± 16	75 ± 11	
		overall	29 ± 6	45 ± 5	34 ± 3	86 ± 9	39 ± 7	58 ± 5	76 ± 7	
		task1	1 ± 3	0 ± 0	0 ± 0	98 ± 7	6 ± 15	0 ± 0	25 ± 11	
		task2	1 ± 4	0 ± 0	0 ± 0	92 ± 16	28 ± 10	72 ± 17	88 ± 9	
		task3	0 ± 0	0 ± 1	0 ± 0	68 ± 27	9 ± 5	32 ± 11	94 ± 6	
	pointmaze-teleport-navigate-v0	task4	0 ± 0	0 ± 0	0 ± 0	66 ± 20	64 ± 17	60 ± 22	25 ± 11	
		task5	5 ± 12	0 ± 0	0 ± 0	19 ± 32	29 ± 28	66 ± 20	81 ± 10	
		overall	1 ± 2	0 ± 0	0 ± 0	68 ± 7	27 ± 10	46 ± 9	65 ± 9	
		task1	1 ± 2	33 ± 12	0 ± 1	0 ± 0	3 ± 3	5 ± 5	25 ± 11	
		task2	4 ± 6	49 ± 2	39 ± 14	8 ± 10	30 ± 23	6 ± 6	25 ± 11	
stitch	pointmaze-medium-stitch-v0	task3	50 ± 4	46 ± 5	31 ± 19	2 ± 5	26 ± 6	39 ± 9	50 ± 13	
		task4	33 ± 13	49 ± 4	42 ± 13	12 ± 16	40 ± 11	24 ± 11	38 ± 12	
		task5	38 ± 6	48 ± 4	9 ± 9	1 ± 2	20 ± 15	17 ± 8	12 ± 9	
		overall	25 ± 3	45 ± 3	24 ± 7	4 ± 4	24 ± 6	18 ± 4	40 ± 4	
		task1	21 ± 29	76 ± 14	56 ± 24	94 ± 13	0 ± 0	77 ± 14	94 ± 6	
	pointmaze-large-stitch-v0	task2	32 ± 35	79 ± 23	26 ± 19	81 ± 34	0 ± 0	61 ± 23	62 ± 12	
		task3	33 ± 34	69 ± 16	0 ± 0	66 ± 29	2 ± 3	82 ± 13	94 ± 6	
		task4	0 ± 0	41 ± 37	0 ± 0	68 ± 32	0 ± 0	92 ± 6	94 ± 6	
		task5	29 ± 37	84 ± 11	22 ± 22	92 ± 9	0 ± 0	59 ± 9	100 ± 0	
		overall	23 ± 18	70 ± 14	21 ± 9	80 ± 12	0 ± 1	74 ± 6	90 ± 7	
pointmaze	pointmaze-giant-stitch-v0	task1	8 ± 13	0 ± 1	56 ± 11	100 ± 1	0 ± 0	3 ± 5	100 ± 0	
		task2	0 ± 0	0 ± 0	0 ± 0	74 ± 37	0 ± 0	0 ± 0	100 ± 0	
		task3	26 ± 28	60 ± 29	98 ± 4	74 ± 23	0 ± 0	59 ± 25	93 ± 7	
		task4	0 ± 0	0 ± 0	0 ± 0	88 ± 32	0 ± 0	1 ± 4	93 ± 7	
		task5	0 ± 0	0 ± 0	0 ± 0	85 ± 22	0 ± 0	0 ± 0	100 ± 0	
		overall	7 ± 5	12 ± 6	31 ± 2	84 ± 15	0 ± 0	13 ± 6	96 ± 2	
	pointmaze-teleport-stitch-v0	task1	0 ± 0	0 ± 0	0 ± 0	99 ± 2	0 ± 0	0 ± 0	100 ± 0	
		task2	0 ± 0	0 ± 0	0 ± 0	80 ± 27	0 ± 0	0 ± 0	100 ± 0	
		task3	0 ± 0	0 ± 0	0 ± 0	3 ± 5	0 ± 0	0 ± 0	94 ± 6	
		task4	0 ± 0	0 ± 0	0 ± 0	63 ± 23	0 ± 0	0 ± 0	100 ± 0	
		task5	0 ± 0	0 ± 0	0 ± 0	4 ± 8	0 ± 0	0 ± 0	100 ± 0	
gridworld	gridworld-medium-v0	overall	0 ± 0	0 ± 0	0 ± 0	50 ± 8	0 ± 0	0 ± 0	99 ± 1	
		task1	28 ± 20	34 ± 14	0 ± 0	0 ± 0	0 ± 0	24 ± 13	75 ± 11	
		task2	13 ± 15	41 ± 8	12 ± 14	7 ± 7	0 ± 0	23 ± 11	12 ± 9	
	gridworld-large-v0	task3	48 ± 8	50 ± 5	47 ± 2	15 ± 13	0 ± 0	46 ± 9	0 ± 0	
		task4	40 ± 16	50 ± 6	46 ± 5	19 ± 12	8 ± 8	46 ± 5	12 ± 9	
		task5	29 ± 16	48 ± 5	21 ± 7	1 ± 3	13 ± 13	31 ± 10	6 ± 6	
gridworld	gridworld-large-v0	overall	31 ± 9	44 ± 2	25 ± 3	9 ± 5	4 ± 3	34 ± 4	20 ± 5	

Table 10. Full Results on AntMaze

Environment Type	Dataset Type	Dataset	Task	GCBC	GCIVL	GCIQL	QRL	CRL	HIQL	ALPS	
antmaze	navigate	antmaze-medium-navigate-v0	task1	35 ± 9	81 ± 10	63 ± 9	93 ± 2	97 ± 1	94 ± 2	94 ± 6	
			task2	21 ± 7	85 ± 5	78 ± 8	90 ± 5	95 ± 2	97 ± 1	100 ± 0	
			task3	28 ± 6	60 ± 13	71 ± 8	86 ± 6	92 ± 3	96 ± 2	94 ± 6	
			task4	28 ± 7	42 ± 25	59 ± 12	83 ± 4	94 ± 5	96 ± 2	94 ± 6	
			task5	37 ± 10	92 ± 3	85 ± 7	88 ± 8	96 ± 2	96 ± 2	94 ± 6	
		overall	29 ± 4	72 ± 8	71 ± 4	88 ± 3	95 ± 1	96 ± 1	95 ± 4		
		antmaze-large-navigate-v0	task1	6 ± 3	16 ± 12	21 ± 6	71 ± 15	91 ± 3	93 ± 3	88 ± 9	
			task2	16 ± 4	5 ± 6	25 ± 7	77 ± 7	62 ± 14	78 ± 9	81 ± 10	
			task3	65 ± 4	49 ± 18	80 ± 5	94 ± 2	91 ± 2	96 ± 2	100 ± 0	
			task4	14 ± 3	2 ± 2	19 ± 6	64 ± 8	85 ± 11	94 ± 2	100 ± 0	
			task5	18 ± 4	5 ± 2	26 ± 9	67 ± 9	85 ± 3	94 ± 3	100 ± 0	
		overall	24 ± 2	16 ± 5	34 ± 4	75 ± 6	83 ± 4	91 ± 2	94 ± 3		
		antmaze-giant-navigate-v0	task1	0 ± 0	0 ± 0	0 ± 0	1 ± 2	2 ± 2	47 ± 10	56 ± 13	
			task2	0 ± 0	0 ± 0	0 ± 0	17 ± 5	21 ± 10	74 ± 5	38 ± 12	
			task3	0 ± 0	0 ± 0	0 ± 0	14 ± 8	5 ± 5	55 ± 7	75 ± 11	
			task4	0 ± 0	0 ± 0	0 ± 0	18 ± 6	35 ± 9	69 ± 5	94 ± 6	
			task5	1 ± 1	1 ± 1	1 ± 1	18 ± 5	16 ± 10	82 ± 4	56 ± 13	
		overall	0 ± 0	0 ± 0	0 ± 0	14 ± 3	16 ± 3	65 ± 5	68 ± 5		
		antmaze-teleport-navigate-v0	task1	17 ± 5	35 ± 5	26 ± 5	31 ± 6	35 ± 5	37 ± 5	56 ± 13	
			task2	51 ± 5	41 ± 5	58 ± 8	47 ± 22	92 ± 3	66 ± 8	38 ± 12	
			task3	22 ± 3	36 ± 8	31 ± 5	35 ± 6	47 ± 4	37 ± 5	44 ± 13	
			task4	25 ± 5	45 ± 3	33 ± 5	33 ± 6	50 ± 2	30 ± 2	38 ± 12	
			task5	14 ± 6	38 ± 6	26 ± 9	28 ± 8	44 ± 3	41 ± 8	38 ± 12	
		overall	26 ± 3	39 ± 3	35 ± 5	35 ± 5	53 ± 2	42 ± 3	44 ± 5		
		antmaze-medium-stitch-v0	task1	70 ± 33	76 ± 13	17 ± 12	43 ± 20	43 ± 10	92 ± 2	81 ± 10	
			task2	65 ± 19	80 ± 4	22 ± 16	61 ± 12	46 ± 14	94 ± 3	81 ± 10	
			task3	21 ± 15	16 ± 12	41 ± 9	72 ± 29	46 ± 17	95 ± 2	88 ± 9	
			task4	1 ± 2	0 ± 0	32 ± 9	80 ± 9	53 ± 19	93 ± 2	100 ± 0	
			task5	70 ± 33	47 ± 20	34 ± 14	41 ± 18	75 ± 8	95 ± 3	100 ± 0	
		overall	45 ± 11	44 ± 6	29 ± 6	59 ± 7	53 ± 6	94 ± 1	95 ± 4		
		antmaze	task1	2 ± 2	23 ± 9	0 ± 0	7 ± 5	1 ± 1	85 ± 5	81 ± 10	
			task2	0 ± 0	0 ± 0	0 ± 0	10 ± 5	4 ± 4	24 ± 16	94 ± 6	
			task3	15 ± 14	69 ± 6	37 ± 10	73 ± 8	43 ± 11	94 ± 3	88 ± 9	
			task4	0 ± 0	0 ± 0	0 ± 0	1 ± 1	5 ± 5	70 ± 8	100 ± 0	
			task5	0 ± 0	0 ± 0	0 ± 0	1 ± 1	1 ± 2	60 ± 9	81 ± 10	
		stitch	overall	3 ± 3	18 ± 2	7 ± 2	18 ± 2	11 ± 2	67 ± 5	95 ± 2	
		antmaze-large-stitch-v0	task1	0 ± 0	0 ± 0	0 ± 0	0 ± 0	0 ± 0	0 ± 1	88 ± 9	
			task2	0 ± 0	0 ± 0	0 ± 0	0 ± 0	0 ± 0	5 ± 5	94 ± 6	
			task3	0 ± 0	0 ± 0	0 ± 0	0 ± 0	0 ± 0	0 ± 0	94 ± 6	
			task4	0 ± 0	0 ± 0	0 ± 0	0 ± 0	0 ± 0	3 ± 3	81 ± 10	
			task5	0 ± 0	0 ± 0	0 ± 0	2 ± 2	0 ± 0	0 ± 1	100 ± 0	
		overall	0 ± 0	0 ± 0	0 ± 0	0 ± 0	0 ± 0	2 ± 2	92 ± 2		
		antmaze-teleport-stitch-v0	task1	21 ± 13	39 ± 7	12 ± 4	22 ± 6	30 ± 6	44 ± 5	69 ± 12	
			task2	39 ± 12	44 ± 6	18 ± 7	22 ± 6	30 ± 4	42 ± 3	44 ± 13	
			task3	34 ± 12	36 ± 8	18 ± 4	25 ± 7	23 ± 11	26 ± 4	38 ± 12	
			task4	46 ± 6	44 ± 4	18 ± 5	24 ± 9	38 ± 4	26 ± 4	38 ± 12	
			task5	16 ± 14	33 ± 6	17 ± 6	26 ± 5	32 ± 7	40 ± 6	25 ± 11	
		overall	31 ± 6	39 ± 3	17 ± 2	24 ± 5	31 ± 4	36 ± 2	34 ± 9		
		antmaze-medium-explore-v0	task1	3 ± 6	10 ± 8	12 ± 6	1 ± 1	2 ± 2	29 ± 17	100 ± 0	
			task2	1 ± 2	74 ± 9	53 ± 8	1 ± 1	8 ± 6	84 ± 10	100 ± 0	
			task3	1 ± 2	0 ± 0	0 ± 0	3 ± 5	4 ± 6	18 ± 24	100 ± 0	
			task4	0 ± 0	0 ± 0	0 ± 0	0 ± 0	0 ± 0	0 ± 0	100 ± 0	
			task5	3 ± 4	10 ± 6	0 ± 0	1 ± 1	2 ± 2	52 ± 27	100 ± 0	
		overall	2 ± 1	19 ± 3	13 ± 2	1 ± 1	3 ± 2	37 ± 10	100 ± 0		
		explore	task1	0 ± 0	37 ± 12	1 ± 1	0 ± 0	0 ± 1	1 ± 3	100 ± 0	
			task2	0 ± 0	0 ± 0	0 ± 0	0 ± 0	0 ± 0	0 ± 0	81 ± 10	
			task3	0 ± 0	12 ± 6	1 ± 1	0 ± 0	1 ± 1	18 ± 24	88 ± 9	
			task4	0 ± 0	0 ± 0	0 ± 0	0 ± 0	0 ± 0	0 ± 0	100 ± 0	
			task5	0 ± 0	0 ± 0	0 ± 0	0 ± 0	0 ± 0	0 ± 0	81 ± 10	
		overall	0 ± 0	10 ± 3	0 ± 0	0 ± 0	0 ± 0	4 ± 5	91 ± 13		
		antmaze-large-explore-v0	task1	2 ± 2	32 ± 4	0 ± 1	0 ± 0	2 ± 1	32 ± 11	62 ± 12	
			task2	0 ± 0	2 ± 4	8 ± 6	0 ± 1	5 ± 4	33 ± 17	50 ± 13	
			task3	4 ± 3	48 ± 3	13 ± 8	4 ± 4	47 ± 6	34 ± 16	56 ± 13	
			task4	2 ± 2	47 ± 5	14 ± 8	4 ± 4	16 ± 12	37 ± 19	38 ± 12	
			task5	4 ± 2	31 ± 2	2 ± 1	3 ± 3	28 ± 5	34 ± 14	12 ± 9	
		overall	2 ± 1	32 ± 2	7 ± 3	2 ± 2	20 ± 2	34 ± 15	46 ± 6		

Table 11. Full Results on HumanoidMaze

Environment Type	Dataset Type	Dataset	Task	GCBC	GCIVL	GCIQL	QRL	CRL	HIQL	ALPS
humanoidmaze	navigate	humanoidmaze-medium-navigate-v0	task1	4 ± 1	22 ± 5	23 ± 6	12 ± 7	84 ± 3	95 ± 2	93 ± 7
			task2	8 ± 4	42 ± 8	49 ± 6	25 ± 8	80 ± 5	96 ± 2	86 ± 10
			task3	12 ± 3	15 ± 3	12 ± 6	25 ± 10	43 ± 11	79 ± 6	93 ± 7
			task4	2 ± 1	0 ± 0	1 ± 0	16 ± 7	5 ± 5	75 ± 6	100 ± 0
			task5	12 ± 4	40 ± 8	51 ± 8	29 ± 12	87 ± 7	97 ± 1	93 ± 7
		overall	8 ± 2	24 ± 2	27 ± 2	21 ± 8	60 ± 4	89 ± 2	86 ± 6	
		humanoidmaze-large-navigate-v0	task1	1 ± 1	6 ± 2	3 ± 2	3 ± 2	36 ± 11	67 ± 4	56 ± 13
			task2	0 ± 0	0 ± 0	0 ± 0	0 ± 0	0 ± 0	2 ± 3	25 ± 11
			task3	3 ± 1	6 ± 2	5 ± 2	17 ± 6	54 ± 17	88 ± 3	62 ± 12
			task4	2 ± 1	0 ± 0	1 ± 1	4 ± 2	23 ± 11	42 ± 11	75 ± 11
			task5	1 ± 1	1 ± 1	1 ± 1	2 ± 1	6 ± 4	47 ± 10	69 ± 12
		overall	1 ± 0	2 ± 1	2 ± 1	5 ± 1	24 ± 4	49 ± 4	54 ± 5	
		humanoidmaze-giant-navigate-v0	task1	0 ± 0	0 ± 0	0 ± 0	0 ± 0	1 ± 1	13 ± 7	50 ± 13
			task2	0 ± 0	1 ± 1	1 ± 1	2 ± 1	9 ± 5	35 ± 11	69 ± 12
			task3	0 ± 0	0 ± 0	0 ± 0	0 ± 0	2 ± 2	11 ± 4	44 ± 13
			task4	0 ± 0	0 ± 0	0 ± 0	0 ± 0	3 ± 2	2 ± 2	75 ± 11
			task5	1 ± 1	0 ± 0	1 ± 1	2 ± 1	1 ± 1	2 ± 2	88 ± 9
		overall	0 ± 0	0 ± 0	0 ± 0	1 ± 0	3 ± 2	12 ± 4	64 ± 9	
		humanoidmaze-medium-stitch-v0	task1	20 ± 7	13 ± 3	12 ± 3	6 ± 5	27 ± 7	84 ± 5	56 ± 13
			task2	49 ± 12	7 ± 2	8 ± 5	13 ± 4	37 ± 7	94 ± 2	69 ± 12
			task3	24 ± 8	25 ± 3	20 ± 7	30 ± 6	40 ± 4	86 ± 4	88 ± 9
			task4	3 ± 2	1 ± 1	2 ± 2	18 ± 5	28 ± 7	86 ± 4	75 ± 11
			task5	49 ± 8	16 ± 3	18 ± 7	22 ± 2	49 ± 5	90 ± 4	75 ± 11
			overall	29 ± 5	12 ± 2	12 ± 3	18 ± 2	36 ± 2	88 ± 2	62 ± 6
		stitch	task1	3 ± 4	2 ± 1	1 ± 1	0 ± 0	0 ± 0	21 ± 5	19 ± 10
			task2	0 ± 0	0 ± 0	0 ± 0	0 ± 0	0 ± 0	5 ± 2	19 ± 10
			task3	20 ± 11	3 ± 2	1 ± 1	16 ± 7	13 ± 3	84 ± 4	69 ± 12
			task4	2 ± 1	1 ± 1	0 ± 1	1 ± 1	4 ± 1	19 ± 4	50 ± 13
			task5	2 ± 2	1 ± 1	0 ± 0	0 ± 0	3 ± 1	12 ± 2	31 ± 12
			overall	6 ± 3	1 ± 1	0 ± 0	3 ± 1	4 ± 1	28 ± 3	35 ± 5
		humanoidmaze-large-stitch-v0	task1	0 ± 0	0 ± 0	0 ± 0	0 ± 0	0 ± 0	1 ± 2	75 ± 11
			task2	0 ± 0	1 ± 1	0 ± 0	1 ± 1	0 ± 0	12 ± 6	62 ± 12
			task3	0 ± 0	0 ± 0	0 ± 0	0 ± 0	0 ± 0	2 ± 2	25 ± 11
			task4	0 ± 0	0 ± 0	0 ± 0	0 ± 0	0 ± 0	1 ± 1	75 ± 11
			task5	0 ± 0	0 ± 0	1 ± 1	1 ± 1	0 ± 1	0 ± 1	94 ± 6
			overall	0 ± 0	0 ± 0	0 ± 0	0 ± 0	0 ± 0	3 ± 2	38 ± 8

 Table 12. Success rates (%) for the six variants of ALPS compared in Section 6 on a subset of the OGBench tasks considered. Results averaged over 8 seeds with standard deviation reported after ±. CEM, π_{prior} , and CEM + π_{prior} are the low-level planning only variants. Dijkstra + CEM and Dijkstra + π_{prior} are the hierarchical planning variants with either CEM or π_{prior} acting as the low-level planner.

Environment	Dataset	CEM	π_{prior}	CEM + π_{prior}	Dijkstra + CEM	Dijkstra + π_{prior}	ALPS
pointmaze	pointmaze-medium-navigate-v0	58 ± 8	19 ± 8	30 ± 7	100 ± 0	46 ± 10	82 ± 10
	pointmaze-large-navigate-v0	19 ± 11	17 ± 10	21 ± 9	100 ± 0	44 ± 17	76 ± 7
	pointmaze-giant-navigate-v0	0 ± 0	0 ± 0	0 ± 0	52 ± 10	64 ± 21	65 ± 9
	pointmaze-medium-stitch-v0	40 ± 13	40 ± 12	46 ± 11	99 ± 3	82 ± 10	90 ± 7
	pointmaze-large-stitch-v0	0 ± 0	12 ± 9	9 ± 9	100 ± 1	93 ± 4	96 ± 2
	pointmaze-giant-stitch-v0	0 ± 0	0 ± 0	0 ± 0	68 ± 8	98 ± 1	99 ± 1
	pointmaze-teleport-navigate-v0	5 ± 5	16 ± 6	20 ± 6	15 ± 8	33 ± 6	40 ± 4
	pointmaze-teleport-stitch-v0	5 ± 6	8 ± 5	9 ± 6	10 ± 10	19 ± 7	20 ± 5
antmaze	antmaze-medium-navigate-v0	0 ± 0	50 ± 10	57 ± 8	0 ± 0	92 ± 5	95 ± 4
	antmaze-large-navigate-v0	0 ± 0	30 ± 11	29 ± 12	0 ± 0	90 ± 4	94 ± 3
	antmaze-giant-navigate-v0	0 ± 0	2 ± 1	2 ± 2	0 ± 0	54 ± 5	68 ± 5
	antmaze-medium-stitch-v0	0 ± 0	50 ± 13	55 ± 12	0 ± 0	92 ± 4	95 ± 4
	antmaze-large-stitch-v0	0 ± 0	14 ± 8	11 ± 7	0 ± 0	93 ± 2	95 ± 2
	antmaze-giant-stitch-v0	0 ± 0	0 ± 0	0 ± 0	0 ± 0	88 ± 3	92 ± 2
	antmaze-medium-explore-v0	0 ± 0	11 ± 6	7 ± 3	47 ± 22	92 ± 4	100 ± 0
	antmaze-large-explore-v0	0 ± 0	1 ± 1	0 ± 0	11 ± 8	43 ± 9	91 ± 13
humanoidmaze	antmaze-teleport-navigate-v0	0 ± 0	35 ± 6	38 ± 6	0 ± 0	44 ± 5	44 ± 5
	antmaze-teleport-stitch-v0	0 ± 0	21 ± 8	24 ± 8	0 ± 0	33 ± 10	34 ± 9
	antmaze-teleport-explore-v0	6 ± 3	4 ± 3	9 ± 5	13 ± 5	38 ± 5	46 ± 6
	humanoidmaze-medium-navigate-v0	0 ± 0	29 ± 12	26 ± 10	0 ± 0	86 ± 6	86 ± 6
	humanoidmaze-large-navigate-v0	0 ± 0	3 ± 2	3 ± 2	0 ± 0	58 ± 6	54 ± 5
	humanoidmaze-giant-navigate-v0	0 ± 0	0 ± 0	0 ± 0	0 ± 0	66 ± 10	64 ± 9
humanoidmaze	humanoidmaze-medium-stitch-v0	0 ± 0	33 ± 8	31 ± 7	0 ± 0	64 ± 6	62 ± 6
	humanoidmaze-large-stitch-v0	0 ± 0	2 ± 2	1 ± 2	0 ± 0	37 ± 5	35 ± 5
	humanoidmaze-giant-stitch-v0	0 ± 0	0 ± 1	0 ± 1	0 ± 0	40 ± 10	38 ± 8